Accepted Manuscript

Fire-resistant design of eccentrically compressed stainless steel columns with constraints

Meijing Liu, Shenggang Fan, Wenjun Sun, Runmin Ding, Ting Zhu

PII: S0379-7112(17)30753-1

DOI: 10.1016/j.firesaf.2018.06.006

Reference: FISJ 2720

To appear in: *Fire Safety Journal*

Received Date: 27 December 2017

Revised Date: 16 April 2018

Accepted Date: 23 June 2018

Please cite this article as: M. Liu, S. Fan, W. Sun, R. Ding, T. Zhu, Fire-resistant design of eccentrically compressed stainless steel columns with constraints, *Fire Safety Journal* (2018), doi: 10.1016/j.firesaf.2018.06.006.

Fire-Resistant Design of Eccentrically Compressed Stainless Steel Columns with Constraints

Meijing Liu [a], Shenggang Fan [b,*], Wenjun Sun [c], Runmin Ding [b], Ting Zhu [b]

[a] Department of Civil Engineering, Southeast University Chengxian College, Nanjing 210088, China
[b] Key Laboratory of Concrete and Prestressed Concrete Structures of Ministry of Education, School of Civil Engineering, Southeast University, Sipailou #2, Zip: 210096, Nanjing, China.
[c] Tus-Design Group Co., Ltd, Suzhou, China

* Corresponding author, Tel.: +86 02583792950; fax: +86 02583792950. E-mail address: 101010393@seu.edu.cn

Abstract: Based on the test results of 7 specimens in fire, the numerical simulation analysis were performed on the fire-resistance performance of the eccentrically compressed stainless steel columns with constraints and the numerical simulation methods were verified. The parametric analysis was carried out to investigate the influence of key factors (such as load ratio, eccentricity, axial constraint stiffness ratio, slenderness ratio, and so on) on the fire-resistance of the eccentrically compressed stainless steel columns with constraints. Based on the existing fire-resistant design methods of unconstrained stainless steel columns, the calculation formula for the buckling temperature of eccentrically compressed stainless steel columns with constraints is proposed, and the relationship between the buckling temperature and failure temperature is obtained. The results show that the fitting formula can better predict the buckling temperature and the post-buckling stage may better improve the fire resistance performance of stainless steel columns. The load ratio, eccentricity and axial constraint stiffness ratio are the key factors that determine the fire-resistance performance of eccentrically compressed stainless steel columns with constraints. The greater the load ratio, eccentricity and axial constraint stiffness ratio, the greater the deviations between the buckling temperature and failure temperature become and the better the fire resistance performance of columns in post-buckling stage. When the slenderness ratio is among 80 - 120, the difference between the buckling temperature and failure temperature is the smallest, and correspondingly, the fire resistance performance of stainless steel column is weakest.

Key words: Stainless steel column; Fire-resistant design method; Eccentrically compressed; Buckling temperature; Failure temperature; Axial constraint stiffness ratio

1. Introduction

Stainless steel has the advantages of good appearance, excellent mechanical properties, strong corrosion resistance, easy maintenance and low life-cycle cost. It is widely applied in the field of construction and has wide application prospects. Stainless steel structures have their irreplaceable applicability in marine engineering. Meanwhile, for the architectural constructions in acid-rain-prone areas, because of its superior corrosion resistance, stainless steel structure has excellent performance in saving building maintenance costs and prolonging construction life-cycle. Stainless steel materials have been gradually developed from decorative components to structural load-bearing main components, which have been widely used in civil engineering [1, 2]. However, in recent years, building fires have occurred frequently, and unprecedented challenges are being faced with regard to the safety of building structures in fire. As a building structural material, stainless steel structures or components often do not use any fire prevention measures due to attempts to obtain a good appearance effect. Therefore, the behaviour response and mechanical behaviour of stainless steel structures in fire are particularly important. Alternately, the structure in fire often has a strong integrity. There are quite complex interactions and internal force redistributions between each component. Therefore, it is of great theoretical value to study the fire resistance performance of stainless steel columns with constraints.

There are many studies on the behaviour response and fire resistance of constrained carbon steel columns in fire. The main contents are the mechanical properties and buckling temperature of constrained steel columns in fire. Neves et al. [3, 4] used the ZWAN program to carry out numerical simulation analysis of the fire resistance of axially constrained steel columns, and a simple analysis model of the fire resistance of steel columns is proposed. Ali et al. [5] conducted a fire test on 37 axially constrained steel columns to investigate the effects of slenderness ratio, axial constraint stiffness ratio and load ratio on the fire resistance of steel columns. The results show that with the increase of axial constraint stiffness, the additional axial force increases and the refractory time decreases; with the increase of the load ratio, the additional axial force decreases. Simms and Randall [6, 7] analyzed the results of the fire tests of 37 constrained steel columns, and the calculation formula of the additional axial force of steel columns was proposed. Wang [8] analyzed the effects of axial stiffness ratio, load ratio and slenderness ratio on the fire resistance of axially constrained steel columns. Tan et al. [9] conducted a series of fire tests on constrained steel columns to investigate the effects of slenderness ratio and axial constraint stiffness ratio. The results show that the axial constraint stiffness reduces the critical temperature of steel columns. Wang and Li et al. [10-14] carried out a fire resistance test and numerical simulation analysis of two full-scale constrained steel columns and the formula for the buckling temperature and failure temperature of constrained steel columns is proposed. Ge [15] performed a fire test and numerical simulation analysis on Q460 high-strength steel columns with constraints, the results show that the post-buckling performance of steel columns will be significantly improved its fire resistance performance.

The above researches mainly focus on the fire resistance performance of the carbon steel columns with constraints. However, stainless steel takes on a complicated stress-stain relation according to its strong nonlinearity, low proportional limit, unapparent yield platform, anisotropy and strain hardening property. The mechanical properties of stainless steel differ significantly from those of carbon steel owing to variations in the chemical composition of materials. The fire-resistant design methods for carbon steel cannot be used for stainless steel without modification [16]. This has implications for strength and stiffness retention and thermal expansion, influencing the response of individual structural members and structural assemblages [17]. In comparison with carbon steel, stainless steel generally offers superior strength and stiffness retention at elevated temperatures owing to the beneficial effects of the alloying elements but also greater thermal expansion. The ability of a material to retain strength and stiffness at elevated temperatures is crucial for the creation of fire-resistant structures. An investigation of the effect of stress-strain relationships on the fire performance of a member indicated that the behaviour of such a member is very sensitive to the stress condition relative to the temperature-reduced proportional limit and yield stress [18]. Hence, the mechanical properties of stainless steel columns with constraints in a fire are different from those of carbon steel columns.

The following related studies concern the fire-resistant design method of stainless steel columns. A simplified method for calculating the ultimate bearing capacity of stainless steel columns at elevated temperature is given in the European Code (EN1993-1-2 / EN1993-1-4) [19, 20] and the European Design Guidance Manual (2017) [21]. Ala Outinen and Oksanen [22, 23] studied compressed stainless steel members in fire, investigated the influence of multiple parameters on their performance, and the relevant design methods and suggestions were given. Uppfeldt et al. [24, 25] conducted fire tests on six axially compressed short columns with square sections and both ends just connected. Numerical simulation of the fire resistance of stainless steel columns was carried out, and a method for the fire resistance of stainless steel columns is proposed. Gardner and Baddoo [26] carried out a full-scale fire test on 6 axially compressed stainless steel columns, and numerical simulation and parametric analysis were performed to propose relevant design recommendations and methods. Gardner and Ng [27, 28] investigated the effects of parameters such as the slenderness ratio and load level on the fire resistance of stainless steel columns, and the results show that the slenderness ratio and load level are the main influence factors on the critical temperature of stainless steel columns in fire. To and Young [29] evaluated the fire resistance of stainless steel columns with rectangular and circular sections, and two methods for the fire-resistant design of stainless steel columns were put forward. Lopes et al. [30] conducted a numerical simulation analysis of the mechanical properties of stainless steel bending members with welded H-shaped sections in fire, and some amendments were proposed for the fire-resistant design method in the European Code [19,20]. Tondini et al. [31] conducted fire tests on 3 EN 1.4003 ferritic stainless steel long column specimens, and the results show that the temperature gradient along the length of column is the key influence factor on the failure mode of stainless steel columns in fire. Ding and Fan et al. [32-34] conducted fire resistance tests on 6 axially compressed and two eccentrically compressed austenitic stainless steel columns, and the fire-resistant design method of axially compressed stainless steel columns without constraints and fire-resistant design recommendations for eccentrically compressed stainless steel columns were proposed. Fan et al. [35] carried out parametric analysis on the ultimate bearing capacity of stainless steel columns with H-shaped sections in fire, and the results show that the slenderness ratio and section size of the members are the main influence factors of the fire resistance of stainless steel columns with H-shaped sections.

Based on the existing fire test results of 7 eccentrically compressed stainless steel columns with constraints, numerical simulation and parametric analysis of the fire resistance of stainless steel columns were carried out. The influences of the initial imperfections, load ratio, axial constraint stiffness ratio, slenderness ratio, eccentricity and material enhanced strength of corner area on the fire resistance of stainless steel columns were investigated. According to the fire-resistant design method of unconstrained stainless steel columns in the European Code (EN l993-l-2) [19, 20] and the European Design Guidance Manual (2017) [21], the numerical simulation analysis for the fire-resistant design of eccentrically compressed stainless steel columns with constraints were performed. The equivalent principle was adopted, which the bearing capacity of eccentrically compressed stainless steel columns with constraints is the same as that of unconstrained eccentrically compressed stainless steel columns under the condition of component buckling in a fire.Finally, the formula of the buckling temperature of eccentrically compressed stainless steel columns with constraints is proposed, and the relationship between buckling temperature and failure temperature is obtained.

2. Numerical simulation analysis

2.1 Analytical method

There are two main types of thermo-mechanical coupling analysis: direct thermo-mechanical coupling analysis and successive thermo-mechanical coupling analysis. Direct thermo-mechanical coupling analysis is typically used to study the object for which the mutual influence between temperature field and stress field is obvious, and Successive thermo-mechanical coupling analysis can be used to investigate the object for which the stress field is greatly affected by the temperature field while the temperature field is little affected by the stress field.

The eccentrically compressed stainless steel column with constraints is mainly subjected to the combined action of external load and high temperature in fire. It can be seen that the temperature field has a great influence on the stress field, but the stress field has no effect on the temperature field, for the eccentrically compressed stainless steel column with constraints. Therefore, the method of successive thermo-mechanical coupling analysis is adopted as the fire resistance of eccentrically compressed stainless steel columns with constraints.

The finite element software ABAQUS [36] was used to perform the numerical simulation analysis on the fire resistance of eccentrically compressed stainless steel columns with constraints. The existing 7 test specimens were selected as the analytical object.

The fire tests were conducted using a horizontal fire furnace test system. The dimension of the furnace chamber was 2.4 m × 3.4 m × 4.25 m. 8 craters and eight thermocouples were set up in the furnace chamber, which were used to heat and control the temperature of the fire furnace. The furnace chamber was heated according to the ISO-834 standard heating curve. The horizontal loading system mainly includes a horizontal loading reaction frame and a restrained steel beam. The horizontal loading reaction frame provided the main support point for the test loading and was needed to meet the force self-balance. The restrained steel beam provided axial restraint stiffness for the test specimen. The test load was applied to the restrained steel beam using a hydraulic jack. The plane layout of the horizontal loading system is shown in Fig. 1. The specimens are made of austenitic stainless steel S30408, and the detailed dimensions are shown in Table 1. Considering the uniform load applied to the end section and the realization of the eccentric load, a 30-mm-thick steel end plate was welded at both ends of the test specimen. The material of the end plate was Q235B. Two ear plates were welded vertically at the stainless steel end plate. Each ear plate was connected to the horizontal reaction frame and restrained steel beam with a hinge pin, simulating the hinged support at both ends of the test specimen.

The axial constraint stiffness ratio β is the ratio of bending stiffness of restrained steel beam k_b (when the concentrated load is applied to the mid-span of the beam) to the axial stiffness k_c at room temperature, as detailed in Eqs. (1) ~ (3).

$$\beta = \frac{k_{\mathrm{b}}}{k_{\mathrm{c}}} \quad (1)$$

$$k_{\mathrm{b}} = \frac{48E_{\mathrm{b}}I_{\mathrm{b}}}{l_{\mathrm{b}}^{3}} \quad (2)$$

$$k_{\mathrm{c}} = \frac{E_{\mathrm{c}}A_{\mathrm{c}}}{l_{\mathrm{c}}} \quad (3)$$

Where E_{b} and E_{c} are the elastic modulus of the restrained steel beam and the eccentrically compressed stainless steel column respectively; l_{b} and l_{c} are the effective length of the restrained steel beam and the eccentrically compressed stainless steel column respectively; I_{b} is the section moment of inertia of the restrained steel beam; A_{c} is the sectional area of the axially compressed stainless steel column.

The numerical simulation results were compared with the test results, to verify the feasibility of the numerical simulation method. The code, section size and parameters of specimen in the fire test are shown in Table 1. The specimens were divided into three groups to investigate the effects of different parameters on the fire resistance of eccentrically compressed stainless steel columns with constraints. In the first group, specimens Z2, Z3 and Z4 were used to study the effect of the load ratio. In the second group, specimens Z3, Z5 and Z6 were used to study the effect of the load eccentricity. In the third group, specimens Z1, Z3 and Z7 were used to study the effect of the axial constraint stiffness ratio. For specimens Z1-Z7, the test process and detail test results were shown in Reference [37].

2.2 Analytical Model

The numerical simulation analysis of the fire resistance of eccentrically compressed stainless steel columns with constraints in fire is mainly related to three models: the bearing capacity analysis model at room temperature, the heat transfer analysis model, and the fire resistance analysis model. The bearing capacity analysis model is mainly used to solve the ultimate bearing capacity of columns at room temperature, to determine the load value of stainless steel column in the subsequent fire-resistant analysis. The heat transfer analysis model is used to obtain the temperature curve of stainless steel columns and to provide temperature data for the subsequent fire-resistant analysis. The fire resistance analysis model is used to determine the bearing capacity, buckling temperature and failure mode of stainless steel columns in fire.

2.2.1 Analysis model at room temperature

(1) Geometric model

The bearing capacity analysis model of eccentrically compressed stainless steel columns with constraints is established directly by the finite element software ABAQUS [36]. To improve the accuracy of the finite element model, the model includes the end plates and the connecting ear plate of the test specimen (as shown in Fig. 2). The shell element S4R (4-node unit, each node has 6 degrees of freedom) and the solid element C3D8R are respectively adopted to simulate the specimen, and the end plates and the connecting ear plate at both ends. The boundary condition of the specimen is unilateral hinged at both ends. To accurately simulate the boundary conditions at both ends of the specimens, coupling constraints are created on the contact surfaces between the ear plates and the pin shafts. The restrained ends of the specimens only release the rotational degree of freedom, while the loading ends also need to release the axial translational degree of freedom, allowing axial deformation of the specimens. To get the bearing capacity of specimens accurately and track the descending stage of the load-displacement curve, the arc-length method is adopted. The loading method adopts displacement loading. The loading eccentricity can be adjusted by varying the relative position between the neutral axis and the center of the end plate. The real load adopted should be determined by the load ratio of the specimen. The geometric model of the test specimen is shown in Fig. 3.

(2) Material model

Based on the tensile test results of the mechanical properties of austenitic S30408 stainless steel at room temperature [37], by the processing method of the test results of the mechanical properties of stainless steel proposed by Gardner [38] and the stress-strain formula of stainless steel given by Rasmussen [39], as expressed by Eq. (4), the stress-strain curves and the mechanical properties of stainless steel in the flat and the corner area can be respectively obtained, as shown in Fig. 4.

$$\varepsilon=\begin{cases}\dfrac{\sigma}{E_0}+0.002\left(\dfrac{\sigma}{\sigma_{0.2}}\right)^{\mathrm{n}} & \sigma\subset[0,\sigma_{0.2}]\\[2ex] \dfrac{\sigma-\sigma_{0.2}}{E_{0.2}}+\varepsilon_{\mathrm{u}}\left(\dfrac{\sigma-\sigma_{0.2}}{\sigma_{\mathrm{u}}-\sigma_{0.2}}\right)^{\mathrm{m}}+\varepsilon_{0.2} & \sigma\subset(\sigma_{0.2},\sigma_{\mathrm{u}}]\end{cases} \tag{4}$$

Where ε and σ are the stress and strain of stainless steel; E_0 is the initial elastic modulus; $\sigma_{0.2}$ is the nominal yield strength, the stress corresponding to a residual deformation value of 0.2%; σ_{u} is the ultimate strength of material; $n=\ln(20)/\left[\ln(\sigma_{0.2}/\sigma_{0.01})\right]$ is the hardening index; $m=1+3.5\sigma_{0.2}/\sigma_{\mathrm{u}}$ is the parameter; $\sigma_{0.01}$ is the stress corresponding to a residual deformation value of 0.1%; $E_{0.2}=E_0/\left(1+0.002n\,E_0/\sigma_{0.2}\right)$ is the tangent modulus corresponding to the stress $\sigma_{0.2}$; $\varepsilon_{0.2}=\sigma_{0.2}/E_0+0.002$ is the strain corresponding to the stress $\sigma_{0.2}$; σ_{u} is the ultimate strain.

In the FE analysis model, the mechanical properties of stainless steel in the flat and the corner area adopt the corresponding stress-strain curves in Fig. 4, respectively.

(3) Initial imperfection

The initial overall imperfection s and local imperfections of stainless steel columns should be considered in the analysis model at the same time. The initial overall imperfections are adopted by the measured values, as shown in Table 2, and the local imperfections are calculated according to the recommended formula proposed by Gardner and Nethercot [40], as detailed in Eq. (5).

$$w_{\mathrm{o}} = 0.023t\left(\sigma_{0.2}/\sigma_{\mathrm{cr}}\right) \tag{5}$$

Where w_{o} is the local imperfections amplitude of stainless steel columns; t is the thickness of cross section; σ_{cr} is the elastic buckling stress of cross section, which can be calculated by the program CUFSM [41].

2.2.2 Heat transfer analysis model

(1) Geometric model

For the eccentrically compressed stainless steel columns with constraints, the establishment, geometric size and meshing of the heat transfer analysis model are exactly the same as those of the bearing capacity analysis model at room temperature. However, there are some differences between the two models, the quadrilateral heat transfer shell element DS4 is adopted to simulate the specimen in the heat transfer analysis model, and it is not necessary to consider the end constraints of the specimen. The transient heat transfer analysis is adopted as the calculation method and the standard ISO834 heating curve is applied in the heating mode.

(2) Thermal parameter

The thermal parameters of stainless steel at elevated temperature are the key data in the heat transfer analysis model. The thermal parameters of stainless steel mainly include the thermal conductivity, specific heat coefficient and thermal expansion coefficient, which can be determined by the method in the European Code (EN l993-l-2) [19]. According to the existing research results

[27], in a standard fire scenario, the other thermal parameters are selected as follows: the thermal radiation coefficient $\varepsilon_{\mathrm{m}} = 0.2$, convective heat transfer coefficient $h = 35\mathrm{W}/\left(\mathrm{m}^2 \cdot {}^{\mathrm{o}}\mathrm{C}\right)$, flame radiation coefficient $\varepsilon_{\mathrm{f}} = 1.0$, and Boltzmann constant $KB = 5.67\times10^{-8}\ \mathrm{W}/\left(\mathrm{m}^2 \cdot \mathrm{K}^4\right)$.

2.2.3 Fire resistance analysis model

(1) Geometric model

The establishment, geometric size, meshing, computing element and boundary conditions of the fire resistance analysis model are all the same as those of the bearing capacity analysis model at room temperature. In the fire resistance analysis model, the loading method is loaded by force, and the loading rate is consistent with that in the fire test. To ensure that the analysis results of temperature field are accurately introduced into the fire resistance analysis model, the computing method and calculating parameter in the fire resistance analysis model are completely consistent with those of heat transfer analysis model.

(2) Material model at elevated temperature

According to the tensile test results of the mechanical properties of the austenitic S30408 stainless steel at elevated temperature [37], and the stress-strain formula of stainless steel at elevated temperature recommended by Chen and Young [16], as expressed by Eq. (6), the stress-strain curves and the mechanical properties of stainless steel in the flat and the corner area at elevated temperature can be respectively obtained, as shown in Fig. 6.

$$\varepsilon_{\theta} = \begin{cases} \dfrac{\sigma_{\theta}}{E_{\theta}} + 0.002\left(\dfrac{\sigma_{\theta}}{\sigma_{0.2,\theta}}\right)^{\mathrm{n}_{\theta}} & \sigma_{\theta} \subset [0, \sigma_{0.2,\theta}] \\ \dfrac{\sigma_{\theta} - \sigma_{0.2,\theta}}{E_{0.2,\theta}} + \varepsilon_{\mathrm{u},\theta}\left(\dfrac{\sigma_{\theta} - \sigma_{0.2,\theta}}{\sigma_{\mathrm{u},\theta} - \sigma_{0.2,\theta}}\right)^{\mathrm{m}_{\theta}} + \varepsilon_{0.2,\theta} & \sigma_{\theta} \subset (\sigma_{0.2,\theta}, \sigma_{\mathrm{u},\theta}] \end{cases} \tag{6}$$

Where σ_{θ} and ε_{θ} are the stress and strain of stainless steel at the temperature of θ °C; $\sigma_{0.2,\theta}$

is the nominal yield strength of stainless steel at the temperature of θ °C; $\sigma_{u,\theta}$ is the ultimate tensile strength of stainless steel at the temperature of θ °C; E_{θ} and $E_{0.2,\theta}$ are the initial elastic modulus and the tangent modulus corresponding to the stress $\sigma_{0.2,\theta}$ at the temperature of θ °C; $\varepsilon_{0.2,\theta}$ is the plastic strain corresponding to the stress $\sigma_{0.2,\theta}$ at the temperature of θ °C; $\varepsilon_{u,\theta}$ is the ultimate strain of stainless steel at the temperature of θ °C; n_{θ} is the hardening index of stainless steel at the temperature of θ °C, generally $n_{\theta} = 6 + 0.2\theta$; m_{θ} is the modified hardening index of stainless steel at the temperature of θ °C, for EN1.4301 stainless steel (austenitic S304), $m_{\theta} = 2.3 - 0.001\theta$, for EN1.4462 stainless steel, $m_{\theta} = 2.3 - 0.005\theta$.

2.3 Numerical simulation results

According to the above three analysis models, the numerical simulation analysis was performed on the fire resistance of specimens Z1–Z7. The ultimate bearing capacity, temperature curve, deformation curve, buckling temperature, failure temperature and failure mode of specimens were obtained, to verify the accuracy and feasibility of the numerical simulation analysis method.

2.3.1 Ultimate bearing capacity at room temperature

For the specimens Z1–Z7, the results of ultimate bearing capacity are shown in Table 3. The analysis results are compared with the results obtained by Hua X [42], Technical specification for stainless steel structures (CECS410-2015) [43] and European Standard (EN 1993-1-4) [20]. The results show that the numerical simulation results are in good agreement with the results obtained by current specifications and existing literature. It is proved that the analysis model at room temperature can accurately predict the ultimate bearing capacity of eccentrically compressed stainless steel columns with constraints.

2.3.2 Temperature-time curves

The temperature-time curves of specimens obtained by heat transfer analysis and their comparison with the test results are shown in Fig. 7, only presented by partial specimens Z1, Z4 and Z7. In the brackets of Fig. 7, FR means the area exposed to fire in the middle of the specimen, and PR means the fire area protected by rock wool at both ends of the specimen.

It can be seen from Fig. 7 that: (1) for the temperature-time curves in PR area, the analysis results are consistent with the test results; (2) for the temperature-time curves in FR area, the test results are higher than the analysis results in the early stage of heating, and the test results are consistent with the analysis results at the later stage of heating. Finally, the analysis results are higher than the test results in the cooling stage; and (3) for the temperature-curves of specimens, the trend of curves between the analysis results and tests results are similar.

2.3.3 Axial displacement-time curves

According to the results of fire test on 7 eccentrically compressed stainless steel columns with constraints [37], the axial displacement-temperature (or heating time) curve of the specimens shows two stages: pre-buckling stage and post-buckling stage, as shown in Fig. 8. The pre-buckling stage was the stage where the axial deformation of the specimen was transformed from the beginning of the thermal expansion to the maximum value. When the axial expansive deformation of the specimen reached its maximum value, the specimen buckled, and the specimen surface temperature was considered as the buckling temperature T_{bt}. The post-buckling stage was when the axial deformation of the specimen was being transformed from the expanded state to the compressed state (i.e., the maximum axial displacement value) until the axial displacement returned to its initial value (at room temperature). When the axial displacement of the specimen returned to its initial value, the specimen was considered to have failed, and the surface temperature of the specimen was considered as the failure temperature of the specimen T_{f1}.

The axial displacement-time curves of specimens obtained by fire resistance analysis and their comparison with the test results are shown in Fig. 9, only presented by partial specimens Z1, Z4 and Z7. It can be seen from Fig. 9 that: (1) the difference between the test results and the analysis results is small before the buckling of specimen, and the test results are slightly higher than the analysis results; (2) the test results are different from the analysis results after the buckling of specimen; (3) for the axial displacement-time curves of specimens, there are some differences between the test results and the analysis results, but the two results are generally in good agreement.

2.3.4 Mid-span lateral displacement-time curve of specimens

The mid-span lateral displacement-time curves of specimens obtained by heat transfer analysis and their comparison with the test results are shown in Fig. 10, only presented by partial specimens Z1, Z4 and Z7. The following conclusions can be drawn from Fig. 10: (1) for the change trend of lateral displacement-time curves, the analysis results are consistent with the test results; the lateral displacement increases slowly with the heating time before the buckling of specimen, and increases rapidly after the buckling of specimen; the lateral displacement increases slowly again untill the failure of specimens; (2) for the value of lateral displacement, there are some differences between the analysis results and the test results; the test value is larger than the analysis value before the buckling of specimen, and the test value is less than the analysis value after the buckling of specimen; (3) For the heating time occurred the buckling of specimen, there is a sudden increase of displacement in the lateral displacement-time curves of each specimen, and the time obtained by the analysis result is earlier than that of the test result; and (4) for the lateral displacement-time curves of specimens, the analysis results are different from the test results at the later stage of heating, but the two results are generally in good agreement.

2.3.5 Axial force-time curves

For the eccentrically compressed stainless steel columns with constraints in fire, the specimens experience the expansion deformation at initial stage of heating up, and an internal additional axial force is generated in the specimen. The additional axial force will reach its maximum close to the buckling of specimen. After the buckling of specimen is occurred, the axial force will gradually decrease with the increase of lateral displacement of specimen. The limit state is adopted as the failure of specimen in fire, which the axial force of specimen is restored to the initial value, corresponding with the failure temperature T_{f1} of specimen, as shown in Fig. 8.

The axial force-time curves of specimens obtained by heat transfer analysis and their comparison with the test results are shown in Fig. 11, only presented by partial specimens Z1, Z4 and Z7. The following conclusions can be drawn from Fig. 11: (1) for each specimen, the maximum value of axial force is approximately twice the value of initial axial force at room temperature; and (2) for the axial force-time curves, the analysis results are in good agreement with the test results.

2.3.6 Buckling temperature and failure temperature

For the buckling temperature and failure temperature of specimens Z1–Z7, the test results and analysis results are shown in Table 4. The following conclusions can be drawn from Table 4: (1) for the buckling temperature and the failure temperature of each specimen, the test results are slightly different from the analysis results, and the maximum value of the deviation is within 10%; (2) the buckling temperature of a specimen decreases with the increase of the load ratio, axial stiffness ratio and eccentricity; (3) the failure temperature of a specimen decreases gradually with the increase of the load ratio and the decrease of the eccentricity, but the axial stiffness ratio has a small effect on the failure temperature; and (4) for the buckling temperature and the failure temperature of specimens, the test results are basically consistent with the analysis results.

2.3.7 Failure mode of specimens

Fig. 12 shows only the analysis results and test results for the failure modes of specimens Z1 and Z7. The failure mode of specimens Z2–Z6 is exactly the same as that of specimen Z1 and will not be repeated. Fig. 12 indicates that (1) for the failure mode of specimen Z1, the analysis results are in good agreement with the test results, which are presented as the integrated bending-buckling mode, and the maximum value of lateral displacement occurs at the mid-span section. (2) for the failure mode of specimen Z7, the analysis results are consistent with the test results, which is presented as the coupling mode between integrated bending-buckling and local buckling, and the local buckling occur at the mid-span section.

For eccentrically compressed stainless steel columns with constraints, there are two types of failure mode in fire. The first type is integrated bending-buckling mode, as shown in Fig. 12 (a). The second type is the coupling mode between integrated bending-buckling and local buckling, as shown in Fig. 12 (b). The numerical simulation method can successfully simulate the failure mode of eccentrically compressed stainless steel columns with constraints in fire.

3. Parametric analysis

3.1 Parameter selection

According to the existing research results [28,37,44], the key influence parameters of the fire resistance of stainless steel columns with constraints are as follows: initial imperfection w_0, load ratio n, axial constraint stiffness ratio β, slenderness ratio λ, eccentricity e and material enhanced strength of corner area. The methods of numerical simulation analysis in Section 2.2 are adopted as the parametric analysis of the fire resistance of eccentrically compressed stainless steel columns with constraints, and the heating mode abides by the standard ISO834 heating curve.

The grouping and basic parameters of selected specimens are shown in Table 5. The specimens are divided into 6 groups, with a total of 40 specimens, which are respectively used to investigate the influence of initial imperfection, load ratio, axial constraint stiffness ratio, slenderness ratio, eccentricity, material enhanced strength of corner area on the fire resistance of eccentrically compressed stainless steel columns with constraints. The section size of specimen is selected as RHS 140 mm×120 mm×5 mm, and the length of specimen is 3300 mm.

3.2 Initial imperfections

Gardner and Nethercot [40] carried out numerical simulation analysis of the bearing capacity of a series of stainless steel columns with different initial imperfections. The amplitudes of initial imperfections are L_0/1000, L_0/2000 and L_0/5000, respectively. The results show that the analysis results are in good agreement with the test results when the amplitudes of initial imperfection is L_0/2000. Ng and Gardner [28] numerically simulate the influence of initial imperfection on the critical temperature of stainless steel columns in a fire, and the results show that the analysis results are consistent with the test results when the amplitudes of initial imperfection is L_0/2000.

To investigate the influence of initial imperfection on the fire resistance of eccentrically compressed stainless steel columns with constraints, the amplitudes of imperfections of specimens P1-1~P1-5 are 0, L_0/5000, L_0/2000, L_0/1000, and L_0/500, respectively. The code and other parameters of specimens are shown in Table 5.

For specimens P1-1~P1-5 in Table 5, the axial displacement-time curves and axial force-time curves are respectively shown in Fig. 13 (a) and (b). The axial force ratio in Fig. 13(b) refers to the ratio of the actual axial force N_F at elevated temperature to the ultimate bearing capacity N_u at room temperature. The following conclusions can be drawn from Fig. 13: (1) the axial deformation-time curves and axial force ratio-time curves of specimens are basically coincident at the initial stage of heating up; and (2) after the buckling of specimen is occurred, the larger the initial imperfections is, the lower the peak points of axial displacement-time curves and axial force ratio-time curves are.

The curves of the buckling temperature and failure temperature with the amplitudes of initial imperfections of specimen are shown in Fig. 14 (a), and the curves of the maximum axial displacement and axial force ratio with the amplitudes of initial imperfections are shown in Fig. 14 (b). Fig. 14 indicates that: (1) the amplitudes of initial imperfections w_0 has little effect on the buckling temperature and failure temperature of eccentrically compressed stainless steel columns with constraints; and (2) the maximum axial displacement and axial force ratio of specimen decrease linearly with the increase of the initial imperfections.

The analysis results show that the initial imperfection has little effect on the fire resistance of eccentrically compressed stainless steel columns with constraints. Thus, the amplitude of initial imperfection is selected as $w_0 = L_0/2000$ in the subsequent analysis.

3.3 Load ratio

Fig. 15 (a) and (b) show the axial displacement-time curves and axial force-time curves of specimens P2-1~P2-10, respectively. The following conclusions can be drawn from Fig. 15: (1) the peak points of the axial displacement-time curves cut down with the increase of the load ratio, the time of heating up corresponding to the peak point is shortened, and the descending branch of the curve becomes steep. (2) Specimens with different load ratios have different failure modes. For the specimens (P2-9 and P2-10) with load ratio $n = 0.8$ and $n = 0.9$, after the buckling of the specimens, the axial displacements descend rapidly, and the failure occurs immediately. There is no post-buckling stage in displacement-time curves. The failure for this kind of specimens is called the Failure Mode1 (brittle failure). For the specimens (P2-2~P2-7) with load ratio $n = 0.1 \sim 0.7$, after the buckling of the specimens, the axial displacements decrease slowly, and there is post-buckling stage in displacement-time curves. It took a long time from the buckling to the failure of specimen and the specimens have obvious ductility. The failure for this kind of specimens is called the Failure Mode2 (ductile failure). For the specimen (P2-1) with a load ratio $n = 0$, the specimen is always expanded and deformed at elevated temperature. The axial displacement of the specimen cannot be restored to the initial value at room temperature. Therefore, the specimen has no failure temperature. (3) The peak point of the axial force ratio-time curve goes up with increase of load ratio. The shorter the time of heating up corresponding to the peak point is, the steeper the descending branch of the axial force ratio-time curve is. (4) After the failure of specimens, the descending rate of the axial force ratio-time curve gradually slows down. Finally, the value of axial force ratio of all specimens is stabilized at approximately 0.1.

The curves of the buckling temperature and failure temperature with the load ratio are shown in Fig. 16 (a), and the curves of the maximum axial displacement and axial force ratio with the load ratio are shown in Fig. 16 (b). Fig. 16 indicates that: (1) with the increase of the load ratio, the buckling temperature and failure temperature decrease gradually, and the deviation between the two temperatures is reduced; (2) for the specimens with large load ratio ($n \geq 0.8$), the deviation between the two temperatures is almost zero; and (3) with the increase of the load ratio, the maximum axial displacement decreases, and the maximum axial force ratio increases gradually.

The analysis results show that the load ratio is the key external influence factor on the fire resistance and the failure mode of eccentrically compressed stainless steel columns with constraints in fire. For the specimens with large load ratio $n \geq 0.8$, the Failure Mode1 (brittle failure) is occurred; however the Failure Mode2 (ductile failure) is usually present in the specimens with low load ratio $n < 0.8$.

3.4 Axial constraint stiffness ratio

Fig. 17 (a) and (b) show the axial displacement-time curves and axial force-time curves of specimens P3-1~P3-11, respectively. The following conclusions can be drawn from Fig. 17: (1) the peak points of the axial displacement-time curves cut down with the increase of the axial constraint stiffness ratio, the time of heating up corresponding to the peak point is shortened, and the descending branch of the curve flattens out a little bit more gently. (2) Specimens with different axial constraint stiffness ratio have different failure modes. For the specimens with little axial constraint stiffness ratio $\beta = 0 \sim 0.02$, there is no post-buckling stage in displacement-time curves, and the specimens present the Failure Mode1 (brittle failure). However, the Failure Mode2 (ductile failure) is occurred in the specimens with large axial constraint stiffness ratio $\beta = 0.05 \sim 5$. (3) The peak point of the axial force ratio-time curve goes up with increase of the axial constraint stiffness ratio. The shorter the time of heating up corresponding to the peak point is, the flatter the descending branch of the axial force ratio-time curve is. (4) After the failure of specimens, the descending rate of the axial force ratio-time curve gradually slows down. Finally, for the specimens with axial constraint stiffness ratio $\beta = 0.05 \sim 5$, the value of axial force ratio is stabilized at approximately 0.1.

The curves of the buckling temperature and failure temperature with the axial constraint stiffness ratio are shown in Fig. 18 (a), and the curves of the maximum axial displacement and axial force ratio with the axial constraint stiffness ratio are shown in Fig. 18 (b). Fig. 18 indicates that: (1) for the specimens with little axial constraint stiffness ratio $\beta < 1.0$, the buckling temperature decreases rapidly with the increase of the axial constraint stiffness ratio; for the specimens with large axial constraint stiffness ratio $\beta > 2.0$, the buckling temperature does not change with the increase of the axial constraint stiffness ratio, remaining at approximately 100 °C; (2) the influence of the axial constraint stiffness ratio on the failure temperature is small, remaining at approximately 700 °C for all specimens; and (3) for the specimens with axial constraint stiffness ratio $\beta < 1.0$, with the increase of the axial constraint stiffness ratio, the maximum axial displacement decreases and the maximum axial force increases; for the specimens with axial constraint stiffness ratio $\beta > 1.0$, the axial constraint stiffness ratio has little effect on the maximum axial displacement and force ratio.

It can be seen that the axial constraint stiffness ratio has a great influence on the fire resistance and the failure mode of eccentrically compressed stainless steel columns with constraints in fire. For the specimens with large axial constraint stiffness ratio $\beta > 0.05$, the Failure Mode1 (brittle failure) is occurred; however the Failure Mode2 (ductile failure) is usually present in the specimens with low load axial constraint stiffness ratio $\beta \leq 0.02$. For the specimens with the axial constraint stiffness ratio $\beta > 2.0$, the fire resistance is almost independent of the axial constraint stiffness ratio.

3.5 Slenderness ratio

Fig. 19 (a) and (b) show the axial displacement-time curves and axial force-time curves of specimens P4-1~P4-6, respectively. The following conclusions can be drawn from Fig. 19: (1) the peak point of the axial displacement-time curves goes up with the increase of the slenderness ratio, and the time of heating up corresponding to the peak point is shortened. For the specimens with the slenderness ratio $\lambda \leq 80$, the descending branch of the curves is fairly flat; for the specimens with the slenderness ratio $\lambda > 80$, the descending branch of the curves is very steep. (2) The Failure Mode2 (ductile failure) is occurred in the specimens P4-1~P4-6, indicating that the slenderness ratio has little influence on the failure modes of eccentrically compressed stainless steel columns with constraints in fire. (3) There are the similar rules and trends between the axial force ratio-time curves and the axial deformation-time curves for all specimens.

The curves of the buckling temperature and failure temperature with the slenderness ratio are shown in Fig. 20 (a), and the curves of the maximum axial displacement and axial force ratio with the slenderness ratio are shown in Fig. 20 (b). Fig. 20 indicates that: (1) the buckling temperatures of specimens decrease approximately linearly with the increase of the slenderness ratio; (2) for the specimens with little slenderness ratio $\lambda \leq 80$, the failure temperature decreases with the increase of the slenderness ratio; for the specimens with large slenderness ratio $\lambda > 80$, the failure temperature basically remains at approximately 640 °C; (3) for the specimens with slenderness ratio $\lambda \leq 100$, the maximum axial displacement increases with the increase of the slenderness ratio; for the specimens with slenderness ratio $\lambda > 100$, the maximum axial displacement is almost independent of the slenderness ratio; and (4) the maximum axial force ratio increases linearly with the increase of the slenderness ratio.

It can be seen that the slenderness ratio is the key internal influence factor on the fire resistance of eccentrically compressed stainless steel columns with constraints.

3.6 Eccentricity

Fig. 21 (a) and (b) show the axial displacement-time curves and axial force-time curves of specimens P5-1~P5-6, respectively. The following conclusions can be drawn from Fig. 21: (1) the peak points of the axial displacement-time curves and the axial force ratio-time curves cut down with the increase of the eccentricity, and the time of heating up corresponding to the peak point is shortened. The descending branch of the curves is fairly flat. (2) For the specimen with the eccentricity $e = 0$ (axially compressed columns), the specimen present the Failure Mode1 (brittle failure); the Failure Mode2 (ductile failure) is occurred in the specimen with the eccentricity $e > 0$ (eccentrically compressed columns). (3) When the heating time is the same, the larger the eccentricity of the specimen is, the larger the axial force ratio is.

The curves of the buckling temperature and failure temperature with the eccentricity are shown in Fig. 22 (a), and the curves of the maximum axial displacement and maximum axial force ratio with the eccentricity are shown in Fig. 22 (b). Fig. 22 indicates that: with the increase of the eccentricity, the buckling temperature decreases gradually and the failure temperature increases gradually; the maximum axial displacement decreases gradually and the maximum axial force ratio increases gradually.

It can be seen that the eccentricity is a key internal influence factor on the fire resistance of eccentrically compressed stainless steel columns with constraints. The larger the eccentricity is, the lower the buckling temperature is, and the higher the failure temperature is. Additionally, for eccentrically compressed stainless steel columns with constraints, the greater the deviation between the buckling temperature and failure temperature, the longer the post-buckling stage and the better the fire resistance performance of specimen. Therefore, for the fire-resistant design of constrained eccentrically compressed stainless steel columns with a large eccentricity, it is suggested that the post-buckling performance be considered to improve the fire-resistant time.

3.7 Material enhanced strength of corner area

Fig. 23 (a) and (b) show the axial displacement-time curves and axial force-time curves of specimens P6-1 and P6-2, respectively. The following conclusions can be drawn from Fig. 23: (1) the axial deformation-time curves of specimens P6-1 and P6-2 are the same before the buckling of the specimens, and the axial deformation-time curve of specimen P6-1 is higher than that of specimen P6-2 after the buckling of the specimens. In addition, the time of heating up corresponding to the peak point of the axial deformation-time curve of specimen P6-1 is shorter than that of specimen P6-2. (2) The axial force ratio-time curve of specimen P6-2 is slightly higher than that of specimen P6-1 before the buckling of the specimens, and the maximum values of the axial force ratio-time between specimen P6-1 and P6-2 are the same after the buckling of the specimens.

The buckling temperature of specimen P6-1 is higher than that of specimen P6-2, and the failure temperature of P6-1 is higher than that of P6-2. According to the above analysis, it can be found that the material enhanced strength of corner area is beneficial to the fire resistance of eccentrically compressed stainless steel columns with constraints.

4. Fire-resistant design method

The behaviour response of eccentrically compressed stainless steel columns with constraints in fire mainly experiences two stages: the pre-buckling stage and the post-buckling stage, as shown in Fig. 8. Thus, the buckling temperature and failure temperature are two key influence factors on the fire-resistant design of eccentrically compressed stainless steel columns with constraints.

4.1 Calculation method for the buckling temperature

4.1.1 Relationship between the axial force and buckling temperature

According to the results of parametric analysis, the influence factors on the fire resistance of eccentrically compressed stainless steel columns with constraints included mainly the internal parameters (slenderness ratio λ and eccentricity e) and the external parameters (load ratio n and axial constraint stiffness ratio β). For eccentrically compressed stainless steel columns with constraints, to investigate the buckling temperature and axial force at the time of buckling of column in fire, two groups of specimens were selected according to the different internal parameters, with a total of 9 specimens, which was respectively used to study effects of the slenderness ratio λ and eccentricity e on the fire resistance of specimens. The codes and basic parameters of specimens are shown in Table 6. The finite element models were established, and the critical temperature and axial force at the time of buckling of specimens were obtained. The finite element models were also divided into two types: Group a and Group b, which were mainly used to investigate the effect of the load ratio n and axial constraint stiffness ratio β on the fire resistance of specimens. The codes and basic parameters of finite element models are shown in Table 7, with a total of 153 models.

According the analysis results of the 153 finite element models, for eccentrically compressed stainless steel columns with constraints, the buckling temperature $T_{\mathrm{bl,FEM}}$ and axial force $N_{\mathrm{bl,FEM}}$ under different conditions can be obtained. Meanwhile, for all specimens in Table 6, if both ends of the specimens are unconstrained, the ultimate bearing capacity $N_{\mathrm{u,T}}$ of the specimens at elevated temperatures can be calculated according to the design methods of eccentrically compressed stainless steel columns without constraints in the European Code [19, 20]. In the same coordinate system, the axial force $N_{\mathrm{bl,FEM}}$ -buckling temperature $T_{\mathrm{bl,FEM}}$ curves (eccentrically compressed columns with constraints) and the ultimate bearing capacity $N_{\mathrm{u,T}}$ -temperature T curves (eccentrically compressed columns without constraints) can be drawn, as shown in Fig. 24 (a) and (b), respectively.

It can be seen from Fig. 24 that: (1) for SP1-1~SP1-4 and SP2-1~SP2-5, the axial force $N_{bl,FEM}$ is slightly higher than the ultimate bearing capacity $N_{u,T}$ at the same temperature, but the derivation between $N_{bl,FEM}$ and $N_{u,T}$ is very small. (2) With the increase of the slenderness ratio λ (from specimen SP1-1 to specimen SP1-4) or the increase of the eccentricity (from specimen SP2-1 to specimen SP2-5), the derivation between $N_{bl,FEM}$ and $N_{u,T}$ decreases gradually. Therefore, it is assumed that $N_{bl,FEM}$ is approximately equal to $N_{u,T}$ at the same temperature.

4.1.2 Formula of buckling temperature

It was assumed that the surface temperature of eccentrically compressed stainless steel columns with constraints in fire is T_{bl}. The analysis results in Section 4.1.1 indicate that the axial force $N_{bl,T}$ (eccentrically compressed columns with constraints) is equal to the ultimate bearing capacity $N_{u,T}$ (eccentrically compressed columns without constraints) under the same temperature condition, which is expressed by Eq. (7). Therefore, in case the axial force corresponding to the buckling of specimen was known, the buckling temperature of eccentrically compressed stainless steel columns with constraints can be obtained by Eq. (7), according to the design methods of eccentrically compressed stainless steel columns without constraints in the European Code [19, 20].

$$N_{bl,T} = N_{u,T} \tag{7}$$

The axial force $N_{bl,T}$ is the composition of the initial axial force N_0 at room temperature and the additional axial force $N_{con,T}$ generated by the axial constraint at elevated temperature, as expressed by Eq. (8).

$$N_T = N_0 + N_{con,T} \tag{8}$$

Fig. 25 (a)-(d) show the four mechanics states: the initial state, room temperature state, free expansion state and constraint state, for eccentrically compressed stainless steel columns with constraints in fire.

According to the four mechanics states in Fig. 25, the following formula can be obtained.

$$u_{\mathrm{f}} = \varepsilon_{\mathrm{th}} L + N_0 / k_{\mathrm{c}} \tag{9}$$

$$k_{\mathrm{c,T}} u_{\mathrm{c}} = N_0 + N_{\mathrm{con,T}} \tag{10}$$

$$k_{\mathrm{b}} (u_{\mathrm{f}} - u_{\mathrm{c}}) = N_{\mathrm{con,T}} \tag{11}$$

Where u_{f} is the deviation of length of column under free expansion state and normal temperature state; $\varepsilon_{\mathrm{th}}$ is the linear expansion coefficient corresponding to the temperature T_{bl}; L is the geometric length of column at room temperature; $k_{\mathrm{c}} = EA/L$ is the axial stiffness at room temperature; $k_{\mathrm{c,T}} = k_{\mathrm{E}} EA/L$ is the axial stiffness at room temperature corresponding to the temperature T_{bl}; u_{c} is the deviation of length of column under free expansion state and constraint state; k_{b} is the axial constraint stiffness; E is the initial elastic modulus of stainless steel at room temperature; A is the sectional area of column; k_{E} is the initial elastic modulus reduction factor of stainless steel at elevated temperature.

For eccentrically compressed stainless steel columns with constraints, the formula of the axial force $N_{\mathrm{bl,T}}$ corresponding to the temperature T_{bl} can be obtained by Eqs. (8) ~ (11), as shown in Eq. (12).

$$N_{\mathrm{bl,\,T}} = N_0 + \left(\frac{k_{\mathrm{c,T}} k_{\mathrm{b}}}{k_{\mathrm{c,T}} + k_{\mathrm{b}}}\right)\left(\varepsilon_{\mathrm{th}} L + \frac{N_0}{k_{\mathrm{c}}} - \frac{N_0}{k_{\mathrm{c,T}}}\right) \tag{12}$$

A calculation formula of ultimate bearing capacity of unrestrained eccentrically compressed stainless steel columns in fire at time *t*, with the section temperature being *θ*, was proposed in the Eurocode (EN1993-1-2) [19]. For eccentrically compressed stainless steel columns with Class 1 and

Class 2 cross-sections, Eq. (13) can be used for calculation. For eccentrically compressed stainless steel columns with Class 3 cross-sections, Eq. (14) can be used for calculation. For eccentrically compressed stainless steel columns with Class 4 cross-sections, Eq. (15) can be used.

$$\begin{cases} \dfrac{N_{\mathrm{fi}}}{\chi_{\mathrm{min,fi}} A k_{\mathrm{y},\theta} f_{\mathrm{y}}} + \dfrac{k_{\mathrm{y}} M_{\mathrm{y,fi}}}{W_{\mathrm{pl,y}} k_{\mathrm{y},\theta} f_{\mathrm{y}}} + \dfrac{k_{\mathrm{z}} M_{\mathrm{z,fi}}}{W_{\mathrm{pl.z}} k_{\mathrm{y},\theta} f_{\mathrm{y}}} \le 1 \\ \dfrac{N_{\mathrm{fi}}}{\chi_{\mathrm{z,fi}} A k_{\mathrm{y},\theta} f_{\mathrm{y}}} + \dfrac{k_{\mathrm{LT}} M_{\mathrm{y,fi}}}{\chi_{\mathrm{LT,fi}} W_{\mathrm{pl,y}} k_{\mathrm{y},\theta} f_{\mathrm{y}}} + \dfrac{k_{\mathrm{z}} M_{\mathrm{z,fi}}}{W_{\mathrm{pl,z}} k_{\mathrm{y},\theta} f_{\mathrm{y}}} \le 1 \end{cases} \tag{13}$$

$$\begin{cases} \dfrac{N_{\mathrm{fi}}}{\chi_{\mathrm{min,fi}} A k_{\mathrm{y},\theta} f_{\mathrm{y}}} + \dfrac{k_{\mathrm{y}} M_{\mathrm{y,fi}}}{W_{\mathrm{el,y}} k_{\mathrm{y},\theta} f_{\mathrm{y}}} + \dfrac{k_{\mathrm{z}} M_{\mathrm{z,fi}}}{W_{\mathrm{el.z}} k_{\mathrm{y},\theta} f_{\mathrm{y}}} \le 1 \\ \dfrac{N_{\mathrm{fi}}}{\chi_{\mathrm{z,fi}} A k_{\mathrm{y},\theta} f_{\mathrm{y}}} + \dfrac{k_{\mathrm{LT}} M_{\mathrm{y,fi}}}{\chi_{\mathrm{LT,fi}} W_{\mathrm{el,y}} k_{\mathrm{y},\theta} f_{\mathrm{y}}} + \dfrac{k_{\mathrm{z}} M_{\mathrm{z,fi}}}{W_{\mathrm{el,z}} k_{\mathrm{y},\theta} f_{\mathrm{y}}} \le 1 \end{cases} \tag{14}$$

$$\begin{cases} \dfrac{N_{\mathrm{fi}}}{\chi_{\mathrm{min,fi}} A_{\mathrm{eff}} k_{\mathrm{y},\theta} f_{\mathrm{y}}} + \dfrac{k_{\mathrm{y}} M_{\mathrm{y,fi}}}{W_{\mathrm{eff,y}} k_{\mathrm{y},\theta} f_{\mathrm{y}}} + \dfrac{k_{\mathrm{z}} M_{\mathrm{z,fi}}}{W_{\mathrm{eff,z}} k_{\mathrm{y},\theta} f_{\mathrm{y}}} \le 1 \\ \dfrac{N_{\mathrm{fi}}}{\chi_{\mathrm{z,fi}} A_{\mathrm{eff}} k_{\mathrm{y},\theta} f_{\mathrm{y}}} + \dfrac{k_{\mathrm{LT}} M_{\mathrm{y,fi}}}{\chi_{\mathrm{LT,fi}} W_{\mathrm{eff,y}} k_{\mathrm{y},\theta} f_{\mathrm{y}}} + \dfrac{k_{\mathrm{z}} M_{\mathrm{z,fi}}}{W_{\mathrm{eff,z}} k_{\mathrm{y},\theta} f_{\mathrm{y}}} \le 1 \end{cases} \tag{15}$$

Where N_{fi} is the axial force of eccentrically compressed stainless columns in fire; $M_{\mathrm{y,fi}}$ and $M_{\mathrm{z,fi}}$ are the bending moments caused by eccentric load about y-axis and z-aixs, respectively; $\chi_{\mathrm{min,fi}}$ is the smaller value of in-plane and out-of-plane stability coefficient of component in fire; $\chi_{\mathrm{z,fi}}$ is the out-of-plane stability coefficient of component in fire; $k_{\mathrm{y},\theta}$ is the yield strength reduction factor of stainless steel at high temperature. f_{y} is the yield strength of stainless steel at room temperature; A and A_{eff} are cross-section area and effective cross-section area, respectively; $W_{\mathrm{pl,y}}$, $W_{\mathrm{el,y}}$ and $W_{\mathrm{eff,y}}$ are plastic modulus, elastic modulus and effective section modulus of cross section, respectively. The coefficient k_{LT}, k_{y} and k_{z} can be calculated by Eqs. (16) ~ (18).

$$k_{\mathrm{LT}} = 1 - \frac{\mu_{\mathrm{LT}} N_{\mathrm{fi}}}{\chi_{\mathrm{z,fi}} A k_{\mathrm{y},\theta} f_{\mathrm{y}}} \le 1, \quad \mu_{\mathrm{LT}} = 0.15 \bar{\lambda}_{\mathrm{z},\theta} \beta_{\mathrm{M,LT}} - 0.15 \le 0.9 \tag{16}$$

$$k_{\mathrm{y}}=1-\frac{\mu_{\mathrm{y}}N_{\mathrm{fi}}}{\chi_{\mathrm{y,fi}}Ak_{\mathrm{y},\theta}f_{\mathrm{y}}}\leq 3\,,\quad \mu_{\mathrm{y}}=(1.2\beta_{\mathrm{M,y}}-3)\bar{\lambda}_{\mathrm{y},\theta}+0.44\beta_{\mathrm{M,y}}-0.29\leq 0.8 \tag{17}$$

$$k_{\mathrm{z}}=1-\frac{\mu_{\mathrm{z}}N_{\mathrm{fi}}}{\chi_{\mathrm{z,fi}}Ak_{\mathrm{y},\theta}f_{\mathrm{y}}}\leq 3\,,\quad \mu_{\mathrm{z}}=(2\beta_{\mathrm{M,z}}-5)\bar{\lambda}_{\mathrm{z},\theta}+0.44\beta_{\mathrm{M,z}}-0.29\leq 0.8 \tag{18}$$

Where $\bar{\lambda}_{\mathrm{y},\theta}$ and $\bar{\lambda}_{\mathrm{z},\theta}$ are the regularization slenderness ratio about y-axis and z-aixs of component in fire; $\beta_{\mathrm{M,y}}$ and $\beta_{\mathrm{M,z}}$ are equivalent bending moment coefficient about y-axis and z-aixs of component, for eccentrically compressed components without end moments, $\beta_{\mathrm{M,y}}$ and $\beta_{\mathrm{M,z}}$ should be 1.

According to Eqs. (12) ~ (15), the formula of critical temperature T_{bl} and axial force $N_{\mathrm{bl,T}}$ of eccentrically compressed stainless steel columns with constrains in fire can be obtained.

4.1.3 Verification of formula accuracy

For the 9 specimens in Table 6 and the 153 finite element models in Table 7, the buckling temperature $T_{\mathrm{bl,\,Eq}}$ of specimen under different conditions was calculated according to Eq. (12) and Eqs. (16) ~ (18), and the results were compared with the buckling temperature $T_{\mathrm{bl,\,FEM}}$ calculated by the finite element models, as shown in Table 8 and Table 9. Comparisons between bucking temperatures $T_{\mathrm{bl,\,Eq}}$ and $T_{\mathrm{bl,\,FEM}}$ at different load ratio and different constraint stiffness ratio were respectively shown in Fig. 26 and Fig. 27.

Fig. 26 indicates that: (1) for the specimens (SP1-1 ~SP1-4) with the different slenderness ratios λ, there are smaller deviations between the buckling temperature $T_{\mathrm{bl,\,Eq}}$ and $T_{\mathrm{bl,\,FEM}}$ under the conditions of different load ratios n; when the load ratio $n\leq 0.5$, the buckling temperature $T_{\mathrm{bl,\,Eq}}$ is slightly higher than $T_{\mathrm{bl,\,FEM}}$; when the load ratio $n>0.5$, $T_{\mathrm{bl,\,Eq}}$ is slightly lower than $T_{\mathrm{bl,\,FEM}}$; and (2) for the specimens (SP2-1 ~ SP2-5) with the different eccentricities e, there are some deviations between the buckling temperature $T_{\mathrm{bl,\,Eq}}$ and $T_{\mathrm{bl,\,FEM}}$ under the conditions of different load ratios n; when the eccentricity $e=0$ and load ratio $n \le 0.4$, the buckling temperature $T_{\mathrm{bl,\,Eq}}$ is slightly higher than $T_{\mathrm{bl,\,FEM}}$; the $T_{\mathrm{bl,\,FEM}}$ is greater than $T_{\mathrm{bl,\,Eq}}$ under the other conditions.

Fig. 27 indicates that: (1) for the specimens (SP1-1 ~SP1-4) with different slenderness ratio λ, the buckling temperature $T_{\mathrm{bl,\,Eq}}$ is very close to $T_{\mathrm{bl,\,FEM}}$ under the conditions of different axial constraint slenderness ratio β; when the axial constraint slenderness ratio $\beta \le 0.05$, the deviations between the buckling temperature $T_{\mathrm{bl,\,Eq}}$ and $T_{\mathrm{bl,\,FEM}}$ increases with the increase of axial constraint slenderness ratio β; when the axial constraint slenderness ratio $\beta > 0.05$, the deviations between $T_{\mathrm{bl,\,Eq}}$ and $T_{\mathrm{bl,\,FEM}}$ decreases with the increase of axial constraint slenderness ratio β; and (2) for the specimens (SP2-1 ~ SP2-5) with different eccentricity e, the buckling temperature $T_{\mathrm{bl,\,Eq}}$ is also very close to $T_{\mathrm{bl,\,FEM}}$; when the eccentricity $e=0$, the buckling temperature $T_{\mathrm{bl,\,Eq}}$ is slightly higher than $T_{\mathrm{bl,\,FEM}}$; when the eccentricity $e>0$, $T_{\mathrm{bl,\,Eq}}$ is higher than $T_{\mathrm{bl,\,FEM}}$; the deviations between buckling temperature $T_{\mathrm{bl,\,Eq}}$ and $T_{\mathrm{bl,\,FEM}}$ increases gradually with the increase of the eccentricity e.

4.2 Relationship between buckling temperature and failure temperature

For eccentrically compressed stainless steel columns with constraints, when the load ratio n is relatively small and the axial constraint stiffness ratio β is large, it will take a long time from the buckling to failure of columns, and the Failure Mode2 (ductile failure) is occurred in the columns, as shown in Fig. 8. The deviations between the buckling temperature and the failure temperature can represent the post-buckling performance of columns in fire, which is beneficial to the fire resistance of eccentrically compressed stainless steel columns with constraints.

According to the analysis results of 9 specimens in Table 6 and 153 calculation models in Table 7, the deviation ΔT between the buckling temperature and failure temperature of column can be obtained, as expressed by Eq. (19). The influences of the load ratio and the axial constraint stiffness ratio on the temperature deviation ΔT were respectively shown in Fig. 28 and Fig. 29.

$$\Delta T = T_{\text{fl}} - T_{\text{bl}} \tag{19}$$

Where T_{fl} is the failure temperature of stainless steel column in fire; T_{bl} is the bucking temperature of stainless steel column in fire.

The following conclusions can be drawn from Fig. 28: (1) for the stainless steel columns with the same slenderness ratio or the same eccentricity, the larger the load ratio, the smaller the deviation ΔT between the buckling temperature and failure temperature; (2) for the column with the same load ratio, with the increase of the slenderness ratio, the temperature deviations ΔT decrease first and then increase; when the slenderness ratio $\lambda = 80 \sim 120$, the temperature deviations ΔT is the smallest, and the post-buckling performance of the stainless steel column in fire is the worst at this time; and (3) for the stainless steel columns with the same load ratio, the greater the eccentricity, the larger the temperature deviations ΔT, and the better the post-buckling performance of columns in fire; when the eccentricity $e/h > 0.5$, the increasing rate of the temperature deviations ΔT gradually decreases with the increase of the eccentricity.

According to Fig. 29, it can be obtained that: (1) for the stainless steel columns with the same slenderness ratio, the larger the axial constraint stiffness ratio, the larger the temperature deviations ΔT between the buckling temperature and failure temperature, and the better the post-buckling performance of columns; when the axial constraint stiffness ratio $\beta < 0.01$, the temperature deviations ΔT is close to 0, and the Failure Mode1 (brittle failure) is occurred in columns; when the axial constraint stiffness ratio $\beta > 0.5$, the temperature deviations ΔT is almost constant with increase of the axial stiffness ratio; (2) for the columns with the same axial constraint stiffness ratio, with the increase of the slenderness ratio, the temperature deviations ΔT decrease first and then increase; when the slenderness ratio $\lambda = 80 \sim 120$, the temperature deviations ΔT is the smallest, and the post-buckling performance of the stainless steel column in fire is the worst at this time; (3) for the stainless steel columns with the same eccentricity, the greater the eccentricity, the larger the temperature deviations ΔT, and the better the post-buckling performance of columns in fire; when the axial constraint stiffness ratio $\beta < 0.01$ and the eccentricity $e/h < 0.5$, the temperature deviations ΔT is close to 0, and the Failure Mode1 (brittle failure) is occurred in columns; when the axial constraint stiffness ratio $\beta > 0.5$ and the eccentricity $e/h > 0.5$, the temperature deviations ΔT is almost constant with increase of the axial stiffness ratio; and (4) for the columns with the same axial stiffness ratio, the greater the eccentricity, the larger the temperature deviations ΔT, and the better the post-buckling performance of columns.

According to the comprehensive analysis, for eccentrically compressed stainless steel columns with constraints, the smaller the load ratio, the larger the eccentricity and the larger the axial constraint stiffness ratio, the greater the deviations ΔT between the buckling temperature and failure temperature, and the better the post-buckling performance of columns. With the increase of the slenderness ratio, the temperature deviations ΔT decrease first and then increase. When the slenderness ratio $\lambda = 80 \sim 120$, the temperature deviations ΔT is the smallest, and the post-buckling performance of the stainless steel column in fire is the worst at this time

5. Conclusions

Based on S30408 austenitic stainless steel, the numerical simulation analysis and parametric analysis on the fire resistance of eccentrically compressed stainless steel columns with constraints were carried out, and the buckling temperature and failure temperature of columns in fire were studied. The main conclusions are as follows:

(1) The parametric analysis results show that the load ratio and the axial constraint slenderness ratio are the external influence factors, and the slenderness ratio and the eccentricity are the internal influence factors on the fire resistance of stainless steel columns with constraints.

(2) The mechanics behaviour of eccentrically compressed stainless steel columns with constraints mainly experiences two stages in fire: the pre-buckling stage and the post-buckling stage. There are two main failure modes: Failure mode 1 (brittle failure) and Failure mode 2 (ductile failure), which are occurred in the stainless steel columns with constraints in fire.

(3) An implicit formula for the buckling temperature of eccentrically compressed stainless steel columns with constraints is proposed, and the accuracy of the formula is verified by the results of numerical simulation analysis based on the 153 finite element models.

(4) The influences of various parameters on the deviation between the buckling temperature and failure temperature were investigated. The relationship between buckling temperature and failure temperature is established to facilitate the fire-resistant design of eccentrically compressed stainless steel columns with constraints.

Based on the research results in this paper, further researches on the fire resistant design methods of eccentrically compressed stainless steel columns with constraints and fine constitutive models of stainless steel will be carried out.

Acknowledgments

The authors gratefully acknowledge the financial support of the National Natural Science Foundations of China (No. 51378105 and No. 51578134). The research was supported by Jiangsu

Provincial Forward-Looking Cooperation Foundation of Industry, Education and Research (No. BY2012200). These financial supports are gratefully acknowledged.

References

[1] Zhao O, Afshan S, Gardner L. Structural response and continuous strength method design of slender stainless steel cross-sections, Eng. Struct. 140 (2017) 14–25.
[2] Zhao O, Gardner L, Young B. Behaviour and design of stainless steel SHS and RHS beam-columns, Thin-Walled Struct. 106 (2016) 330–345.
[3] Neves I C. The critical temperature of steel columns with restrained thermal elongation. Fire Safety Journal, 1995; 24(3): 211-227.
[4] Neves I C, Valente J C., Rodrigues J. Thermal restraint and fire resistance of columns. Fire Safety Journal, 2002; 37(8): 753-771.
[5] Ali F, Shepherd P, Randall M. The effect of axial restraint on the fire resistance of steel columns. Journal of Constructional Steel Research, 1998; 45(1-3): 305-306.
[6] Simms W I. An experimental investigation of axially restrained steel columns in fire. Thesis (PhD). London: University of Ulster; 1997.
[7] Randall M J. The effect of axial restraint on the behavior of steel columns in fire. Thesis (PhD). London: University of Ulster; 1998.
[8] Wang Y C. Post-buckling behavior of axially restrained and axially loaded steel columns in fire conditions. Journal of Structural Engineering, 2004; 130(3): 371-379.
[9] Tan K-H, Toh W-S, Huang Z-F, et al. Structural responses of restrained steel columns at elevated temperatures, Part 1: Experiments. Engineering Structures, 2007; 29(8): 1641-1652.
[10] Wang P J, Li G Q. Post-buckling behavior of axially restrained steel columns in fire. Journal of Tongji University (Natural Science), 2008; 36(4): 438-443.
[11] Li G Q, Wang P J, Wang Y C. Practical analysis method for restrained steel columns in fire (I)-restrained columns under axial compression load. China Civil Engineering Journal, 2010; 43(4): 16-22.
[12] Li G Q, Wang P J, Wang Y C. Practical analysis method for restrained steel columns in fire (I I)-restrained columns under combined axial force and bending moment. China Civil Engineering Journal, 2010; 43(4): 23-29.
[13] Li G Q, Wang P J, Wang Y C. Behaviour and design of restrained steel column in fire, Part 1: Fire test. Journal of Constructional Steel Research, 2010; 66(11):1138-1147.
[14] Wang P J, Li G Q, Wang Y C. Behaviour and design of restrained steel column in fire, Part 3: Practical design method. Journal of Constructional Steel Research, 2010; 66(11):1422-1430.
[15] Ge Y. Study on fire resistance of restrained high strength Q460 steel column. Thesis (Master). Chongqing: College of Civil Engineering, Chongqing University; 2012.
[16] Chen J., Young B. Stress-strain curves for stainless steel at elevated temperatures. Engineering Structures, 2006; 28(2), 229-339.
[17] Gardner L. Stainless steel structures in fire. Proceedings of the Institution of Civil Engineers: Structures and Buildings, 2007; 160(3): 129-138.

[18] Buchanen A., Moss P., Seputro J., Welsh R. The effect of stress–strain relationships on the fire performance of steel beams. Engineering Structures 2004; 26(11):1505–1515.
[19] EN1993-1-2. Eurocode 3: Design of steel structures-Part 1.2: General rules—Structural fire design. European Committee for Standardization, CEN, Brussels; 2005.
[20] EN1993-1-4. Eurocode 3: Design of steel structures-Part 1.4: General rules—supplementary rules for stainless steels. European Committee for Standardization, CEN, Brussels; 2006.
[21] Euro Inox/SCI. Design manual for structural stainless steel. 4nd ed. Building series, Vol 4. Euro Inox and the Steel Construction Institute; 2017.
[22] Ala Outinen T., Oksanen T. Stainless steel compression members exposed to fire. VTT research notes 1864. Espoo (Finland); 1997.
[23] Ala Outinen T. Fire resistance of stainless steel structures. In: Proceedings of the second European conference on steel structure (Euro steel 1999).1999; 165-168.
[24] Uppfeldt B. Stainless steel box columns in fire-analysis and design recommendations. Thesis (PhD). Sweden: Division of structural and construction engineering-steel structures， Dept. of Civil and Environmental and Natural Resources Engineering, Luleå Univ. of Technology; 2000.
[25] Uppfeldt B., Ala Outinen T., Veljkovic M. A design model for stainless steel box columns in fire. Journal of Constructional Steel Research, 2006; 64 (10): 1294-1301.
[26] Gardner L., Baddoo N R. Fire testing and design of Stainless Steel Structures. Journal of Constructional Steel Research, 2006; 62(6): 532-543.
[27] Gardner L., Ng K T. Temperature development in structural stainless steel sections exposed to fire. Fire Safety Journal, 2006; 41: 185-203.
[28] Ng K T., Gardner L. Buckling of stainless steel columns and beams in fire. Engineering Structures, 2007; 29: 717-730.
[29] To E C Y., Young B. Performance of cold-formed stainless steel tubular columns at elevated temperatures. Engineering Structures, 2008; 30 (1): 2012-2021.
[30] Lopes N, Vila Real P, da Silva L S, et al. Numerical analysis of stainless steel beam-column in case of fire. Fire Safety Journal, 2012; 50: 35-50.
[31] Tondini N, Rossi B, Franssen J-M. Experimental investigation on ferritic stainless steel columns in fire. Fire Safety Journal, 2013; 62: 238-248.
[32] Ding X F. Experimental investigation of axial compression and eccentric compression stainless steel columns at elevated temperatures. Thesis (Master). Nanjing: School of Civil Engineering, Southeast University; 2013.
[33] Fan S G, Ding X F, Sun W J, et al. Experimental investigation on fire resistance of stainless steel columns with square hollow section. Thin-Walled Structures, 2016; 98 (1): 196-211.
[34] Fan S G, Zhang L Y, Sun W J, et al. Numerical investigation on fire resistance of stainless steel columns with square hollow section under axial compression. Thin-Walled Structures, 2016; 98 (1): 185-195.
[35] Fan S G, Sun W J, Gui H Y, et al. Fire resistance performance analysis of H-section stainless steel column under axial compression. Engineering Mechanics, 2016; 33(6): 154-162.
[36] ABAQUS. ABAQUS/Standard user's manual volumes I-III and ABAQUS CAE Manual, version 6.4. Pawtucket (USA): Hibbitt, Karlsson & Sorensen, Inc.; 2003.

[37] Sun W J. Investigation on fire resistance of stainless steel columns with axial restraint under eccentric compression loads. Thesis (Master). NanJing: School of Civil Engineering, Southeast University; 2016.
[38] Gardner L. A new approach to stainless steel structural design. Thesis (PhD). London: Department of Civil and Environmental Engineering, Imperial College; 2002.
[39] Rasmussen K J R. Full-range stress-strain curves for stainless steel alloys. Journal of Constructional Steel Research 2003; 59(4): 47-61.
[40] Gardner L, Nethercot D A. Numerical modeling of stainless steel structure components-a consistent approach. Journal of Structural Engineering, ASCE 2004; 130(10): 1586~1601.
[41] Li Z, Schafer B.W. Buckling analysis of cold-formed steel members with general boundary conditions using CUFSM: conventional and constrained finite strip methods. Proceedings of the 20th International conference: Special Conference on Cold-Formed Steel Structures (St. Louis). 2010.
[42] Hua X. Theoretical and experimental investigations on the stability of stainless steel beam-columns (Master). NanJing: School of Civil Engineering, Southeast University; 2013.
[43] Standard of China Construction Association. Technical specification for stainless steel structures (CECS 410:2015). Beijing, China Planning Press; 2015.
[44] Lopes N, Vila Real P. Numerical analysis of stainless steel beam-column in case of fire. Fire Safety Journal, 2012, 50:35-50.

Figure captions

Fig. 1 Horizontal loading system

Fig. 2 Detailed dimensions of specimen

Fig. 3 Geometrical model of test specimen

Fig. 4 Stress-strain curves of stainless steel material in flat and corner area at room temperature

Fig. 5 Initial overall imperfection of test specimen
(a) strong axis x direction (b) weak axis y direction

Fig. 6 Stress-strain curves of stainless steel at elevated temperature
(a) flat area (b) corner area

Fig. 7 Temperature-time curves of partial specimens
(a) Specimen Z1 (b) Specimen Z4 (c) Specimen Z7

Fig. 8 Axial displacement-temperature curve of restrained specimen.

Fig. 9 Axial displacement-time curves of partial specimens
(a) Specimen Z1 (b) Specimen Z4 (c) Specimen Z7

Fig. 10 Lateral displacement-time curves of partial specimens
(a) Specimen Z1 (b) Specimen Z4 (c) Specimen Z7

Fig. 11 Axial force-time curves of partial specimens
(a) Specimen Z1 (b) Specimen Z4 (c) Specimen Z7

Fig. 12 Failure modes of specimens Z1 and Z7
(a) specimen Z1 (b) specimens Z7

Fig. 13 Axial displacement (or force ratio)-time curves with different initial imperfections
(a) axial displacement-time curves (b) axial force ratio-time curves

Fig. 14 Effect of initial imperfections on fire resistance of specimens
(a) bucking temperature and failure temperature-initial imperfections curves
(b) axial displacement and axial force ratio-initial imperfections curves

Fig. 15 Axial displacement (force ratio)-time curves of specimens with different load ratio
(a) axial displacement-time curves (b) axial force ratio-time curves

Fig. 16 Effect of load ratio on fire resistance of specimens
(a) bucking temperature and failure temperature-load ratio curves
(b) axial displacement and axial force ratio-load ratio curves

Fig. 17 Axial displacement (force ratio)-time curves of specimens with different axial constraint stiffness ratio
(a) axial displacement-time curves (b) axial force ratio-time curves

Fig. 18 Effect of axial constraint stiffness ratio on fire resistance of specimens
(a) bucking temperature and failure temperature-axial constraint stiffness ratio curves
(b) axial displacement and axial force ratio-axial constraint stiffness ratio curves

Fig. 19 Axial displacement (force ratio)-time curves of specimens with different slenderness ratio
(a) axial displacement-time curves (b) axial force ratio-time curves

Fig. 20 Effect of slenderness ratio on fire resistance of specimens
(a) bucking temperature and failure temperature-slenderness ratio curves
(b) axial displacement and axial force ratio-slenderness ratio curves

Fig. 21 Axial displacement (force ratio)-time curves of specimens with different eccentricity
(a) axial displacement-time curves (b) axial force ratio-time curves

Fig. 22 Effect of eccentricity on fire resistance of specimens
(a) bucking temperature and failure temperature-eccentricity curves
(b) axial displacement and axial force ratio-eccentricity curves

Fig. 23 Effect of material enhanced strength of corner area on fire resistance of specimen
(a) axial displacement-time curves (b) axial force ratio-time curves

Fig. 24 $N_{\mathrm{bl,FEM}}$ - $T_{\mathrm{bl,FEM}}$ curves and $N_{\mathrm{u,T}}$ -T curves under different conditions
(a) Specimens SP1-1~SP1-4 (b) Specimens SP2-1~SP2-5

Fig. 25 Different mechanics states of eccentrically compressed stainless steel columns with constrains in fire

Fig. 26 Comparison between bucking temperatures $T_{\mathrm{bl,\,Eq}}$ and $T_{\mathrm{bl,\,FEM}}$ at different load ratio
(a) specimens SP1-1 ~SP1-4 (b) specimens SP2-1 ~SP2-5

Fig. 27 Comparison between bucking temperatures $T_{\mathrm{bl,\,Eq}}$ and $T_{\mathrm{bl,\,FEM}}$ at different constraint stiffness ratio
(a) specimens SP1-1 ~SP1-4 (b) specimens SP2-1 ~SP2-5

Fig. 28 Influence of slenderness ratio and eccentricity on temperature deviation between buckling temperature and failure temperature at different load ratios
(a) slenderness ratio (b) eccentricity

Fig. 29 Influence of slenderness ratio and eccentricity on temperature deviation between buckling temperature and failure temperature at different axial constraint stiffness ratios
(a) slenderness ratio (b) eccentricity

Tables

Table 1 Code, section size and other parameters of specimens

Specimen code	Section size $h \times b \times t$ / mm×mm×mm	Eccentricity e / mm	Length l_0 / mm	Load ratio n	Axial constraint stiffness ratio β	Ultimate bearing capacity N_u / kN	Actual load N / kN	Section classification
Z1	RHS 120×120×5	20	3300	0.30	5.39%	305.5	94	1
Z2	RHS 140×120×5	20	3300	0.22	4.95%	375.7	83	2
Z3	RHS 140×120×5	20	3300	0.30	4.95%	375.7	116	2
Z4	RHS 140×120×5	20	3300	0.35	4.95%	375.7	133	2
Z5	RHS 140×120×5	30	3300	0.30	4.95%	337.2	104	2
Z6	RHS 140×120×5	40	3300	0.30	4.95%	307.0	94	2
Z7	RHS 160×120×5	20	3300	0.30	4.58%	447.9	138	4

Table 2 Test results of overall imperfection amplitude of specimen

Specimen code	Section size $h \times b \times t$ / mm×mm×mm	Length l_0 / mm	Overall imperfection amplitude / mm		Ratio	
			e_{0x}	e_{0y}	L_0/e_{0x}	L_0/e_{0y}
Z1	RHS 120×120×5	3300	0.87	2.27	3793	1454
Z2	RHS 140×120×5	3300	1.77	1.96	1865	1684
Z3	RHS 140×120×5	3300	1.03	2.04	3205	1618
Z4	RHS 140×120×5	3300	1.81	2.05	1821	1610
Z5	RHS 140×120×5	3300	1.28	0.99	2574	3333
Z6	RHS 140×120×5	3300	2.11	0.52	1561	6346
Z7	RHS 160×120×5	3300	0.48	0.42	6919	7857
Average value			1.34	1.46	3105	3415

Note: e_{0x} is the imperfection amplitude of the strong axis x direction. e_{0y} is the imperfection amplitude of the weak axis y direction, as shown in Fig. 4 (a) and (b), respectively.

Table 3 Analysis results of ultimate bearing capacity of specimens Z1–Z7 at room temperature

Specimen code	N_{FEM} / kN	Hua X		Chinese Code		European Code	
		N_{HX} / kN	N_{FEM} / N_{HX}	N_{CH} / kN	N_{FEM}/N_{CH}	N_{EN} / kN	N_{FEM}/N_{EN}
Z1	305.5	274.4	1.11	283.2	1.08	295.1	1.04
Z2	375.7	348.2	1.08	362.4	1.04	372.8	1.01
Z3	375.7	348.2	1.08	362.4	1.04	372.8	1.01
Z4	375.7	348.2	1.08	362.4	1.04	372.8	1.01
Z5	337.2	299.2	1.13	314.4	1.07	328.9	1.03
Z6	307.0	263.9	1.16	278.5	1.10	295.4	1.04
Z7	447.9	422.6	1.06	434.1	1.03	425.6	1.05

Table 4 Test results and analysis results of bucking temperature and failure temperature

Specimen code	Section size $h \times b \times t$ / mm×mm×mm	Eccentricity e / mm	Load ratio n	Bucking temperature			Ultimate temperature		
				Tests value	Analysis value	ratio	Tests value	Analysis value	ratio
				$T_{bl,T}$ / °C	$T_{bl,F}$ / °C	$T_{bl,T}/T_{bl,F}$	$T_{fl,T}$ / °C	$T_{fl,F}$ / °C	$T_{fl,T}/T_{fl,F}$
Z1	RHS 120×120×5	20	0.30	502	478	1.050	-	641	-
Z2	RHS 140×120×5	20	0.22	570	551	1.034	-	680	-
Z3	RHS 140×120×5	20	0.30	536	520	1.031	-	642	-
Z4	RHS 140×120×5	20	0.35	522	508	1.028	670	612	1.095
Z5	RHS 140×120×5	30	0.30	495	483	1.025	-	669	-
Z6	RHS 140×120×5	40	0.30	486	451	1.078	700	680	1.029
Z7	RHS 160×120×5	20	0.30	557	543	1.026	675	644	1.040

Table 5 Grouping and basic parameters of specimens

Group	Specimen code	Initial imperfection w_0	Load ratio n	Axial constraint stiffness ratio β	Slenderness ratio λ	Eccentricity e	Enhanced strength of corner area	Influence parameter
1	P1-1, P1-2, P1-3, P1-4, P1-5	**0, L_0/5000, L_0/2000, L_0/1000, L_0/500**	0.3	0.05	60	0.14h	Considered	Initial imperfection
2	P2-1, P2-2, P2-3, P2-4, P2-5, P2-6, P2-7, P2-8, P2-9, P2-10	L_0/2000	**0, 0.1, 0.2, 0.3, 0.4, 0.5, 0.6, 0.7, 0.8, 0.9**	0.05	60	0.14h	Considered	Load ratio
3	P3-1, P3-2, P3-3, P3-4, P3-5, P3-6, P3-7, P3-8, P3-9, P3-10, P3-11	L_0/2000	0.3	**0, 0.005, 0.01, 0.02, 0.05, 0.1, 0.2, 0.5, 1, 2, 5**	60	0.14h	Considered	Axial constraint stiffness ratio
4	P4-1, P4-2, P4-3, P4-4, P4-5, P4-6	L_0/2000	0.3	0.05	**40, 60, 80, 100, 120, 140**	0.14h	Considered	Slenderness ratio
5	P5-1, P5-2, P5-3, P5-4, P5-5, P5-6	L_0/2000	0.3	0.05	60	**0, 0.14h, 0.32h, 0.50h, 0.75h, 1.0h**	Considered	Eccentricity
6	P6-1	L_0/2000	0.3	0.05	60	0.14h	Considered	Enhanced strength of corner area
	P6-2						Un-considered	

Note: L_0 is the length, h is the section height.

Table 6 Codes and basic parameters of specimens

Group	Specimen code	Section size $h \times b \times t$ / mm×mm×mm	Length L_0 / mm	Initial Imperfection w_0	Slenderness ratio λ	Eccentricity e
1	SP1-1, SP1-2, SP1-3, SP1-4	RHS 140×120×5	3300	L_0/2000	**40, 80, 120, 160**	h/4
2	SP2-1, SP2-2, SP2-3, SP2-4, SP2-5	RHS 140×120×5	3300	L_0/2000	60	**0, h/4, h/2, 3h/4, h**

Table 7 Codes and basic parameters of finite element models

Group	Model code	Load ratio n	Axial constraint stiffness ratio β	Group	Model code	Load ratio n	Axial constraint stiffness ratio β
1	SPX-Y-a1	**0.1**	0.05	2	SPX-Y-b1	0.3	0.005
	SPX-Y-a2	**0.2**			SPX-Y-b2		0.01
	SPX-Y-a3	**0.3**			SPX-Y-b3		0.02
	SPX-Y-a4	**0.4**			SPX-Y-b4		0.05
	SPX-Y-a5	**0.5**			SPX-Y-b5		0.1
	SPX-Y-a6	**0.6**			SPX-Y-b6		0.2
	SPX-Y-a7	**0.7**			SPX-Y-b7		0.5
	SPX-Y-a8	**0.8**			SPX-Y-b8		1.0
	SPX-Y-a9	**0.9**					

Note: in model code, SPX-Y is specimen code, X can be 1 or 2, Y can be 1,2,3,4 or 5, specimen code as seen in Table 6; a1~a9 represent different load ratio n ; b1~b8 represent different axial constraint stiffness ratio β .

Table 8 Comparisons between bucking temperatures $T_{bl, Eq}$ and $T_{bl, FEM}$ of specimens SP1-1 ~SP1-4 at different load ratio and different constraint stiffness ratio

Load ratio or	SP1-1(λ=40)	SP1-2(λ=80)	SP1-3(λ=120)	SP1-4(λ=160)

constraint stiffness ratio	$T_{bl,Eq}$ / °C	$T_{bl,FEM}$ /°C	Deviation / %	$T_{bl,Eq}$ / °C	$T_{bl,FEM}$ /°C	Deviation / %	$T_{bl,Eq}$ / °C	$T_{bl,FEM}$ /°C	Deviation / %	$T_{bl,Eq}$ / °C	$T_{bl,FEM}$ /°C	Deviation / %
n=0.1	657	655	0.30	569	556	2.28	471	459	2.55	385	365	5.19
n=0.2	606	591	2.48	519	508	2.12	428	421	1.64	347	335	3.46
n=0.3	536	546	-1.87	463	434	6.26	382	356	6.81	308	283	8.12
n=0.4	462	460	0.43	404	388	3.96	328	318	3.05	273	269	1.47
n=0.5	375	393	-4.80	322	311	3.42	277	267	3.61	238	237	0.42
n=0.6	262	277	-5.73	250	252	-0.80	229	239	-4.37	203	221	-8.87
n=0.7	177	201	-13.56	183	185	-1.09	178	169	5.06	158	157	0.63
n=0.8	116	129	-11.21	120	123	-2.50	123	130	-5.69	112	123	-9.82
n=0.9	72	73	-1.39	73	73	0.00	78	73	6.41	76	83	-9.21
β=0.005	820	802	2.20	828	823	0.60	830	823	0.84	808	806	0.25
β=0.01	778	756	2.83	767	756	1.43	738	728	1.36	688	674	2.03
β=0.02	704	696	1.14	664	657	1.05	612	598	2.29	541	516	4.62
β=0.05	536	546	-1.87	463	434	6.26	382	356	6.81	308	283	8.12
β=0.1	383	413	-7.83	304	297	2.30	247	221	10.53	205	182	11.22
β=0.2	255	277	-8.63	207	195	5.80	164	149	9.15	129	130	-0.78
β=0.5	166	175	-5.42	129	123	4.65	100	98	2.00	80	98	-22.50
β=1	128	149	-16.41	99	98	1.01	77	82	-6.49	62	81	-30.65

Table 9 Comparisons between bucking temperatures $T_{bl,\ Eq}$ and $T_{bl,\ FEM}$ of specimens SP2-1 ~SP2-5 at different load ratio and different constraint stiffness ratio

Load ratio or constraint stiffness ratio	SP2-1(e=0)			SP2-2(e=h/4)			SP2-3(e=h/2)			SP2-4(e=3h/4)			SP2-5(e=h)		
	$T_{bl,Eq}$ / °C	$T_{bl,FEM}$ /°C	Deviation / %	$T_{bl,Eq}$ / °C	$T_{bl,FEM}$ /°C	Deviation / %	$T_{bl,Eq}$ / °C	$T_{bl,FEM}$ /°C	Deviation / %	$T_{bl,Eq}$ / °C	$T_{bl,FEM}$ /°C	Deviation / %	$T_{bl,Eq}$ / °C	$T_{bl,FEM}$ /°C	Deviation / %
n=0.1	687	668	2.8	552	542	1.8	472	467	1.1	419	435	-3.8	377	408	-8.2
n=0.2	630	603	4.3	491	491	0.0	418	423	-1.2	366	384	-4.9	326	355	-8.9
n=0.3	560	538	3.9	424	438	-3.3	352	367	-4.3	307	325	-5.9	276	322	-16.7
n=0.4	475	461	2.9	340	345	-1.5	281	301	-7.1	251	270	-7.6	227	244	-7.5
n=0.5	372	384	-3.2	251	272	-8.4	213	232	-8.9	194	213	-9.8	180	199	-10.6
n=0.6	245	265	-8.2	176	192	-9.1	155	171	-10.3	145	162	-11.7	136	154	-13.2
n=0.7	153	172	-12.4	111	134	-20.7	99	118	-19.2	97	112	-15.5	95	108	-13.7
n=0.8	85	127	-49.4	66	108	-63.6	62	97	-56.5	63	89	-41.3	63	87	-38.1
n=0.9	38	76	-100.0	24	60	-150.0	24	57	-137.5	28	56	-100.0	31	56	-80.6
β=0.005	823	828	-0.6	782	792	-1.3	757	767	-1.3	738	751	-1.8	723	742	-2.6
β=0.01	785	790	-0.6	720	729	-1.3	682	699	-2.5	654	667	-2.0	629	657	-4.5
β=0.02	714	718	-0.6	625	634	-1.4	564	580	-2.8	514	540	-5.1	477	534	-11.9
β=0.05	560	538	3.9	424	438	-3.3	352	367	-4.3	307	325	-5.9	276	322	-16.7
β=0.1	406	378	6.9	278	267	4.0	231	244	-5.6	204	232	-13.7	184	229	-24.5
β=0.2	271	246	9.2	190	188	1.1	158	164	-3.8	139	155	-11.5	125	152	-21.6
β=0.5	175	164	6.3	122	128	-4.9	100	118	-18.0	89	105	-18.0	81	103	-27.2
β=1	135	123	8.9	94	108	-14.9	79	98	-24.1	70	87	-24.3	64	87	-35.9

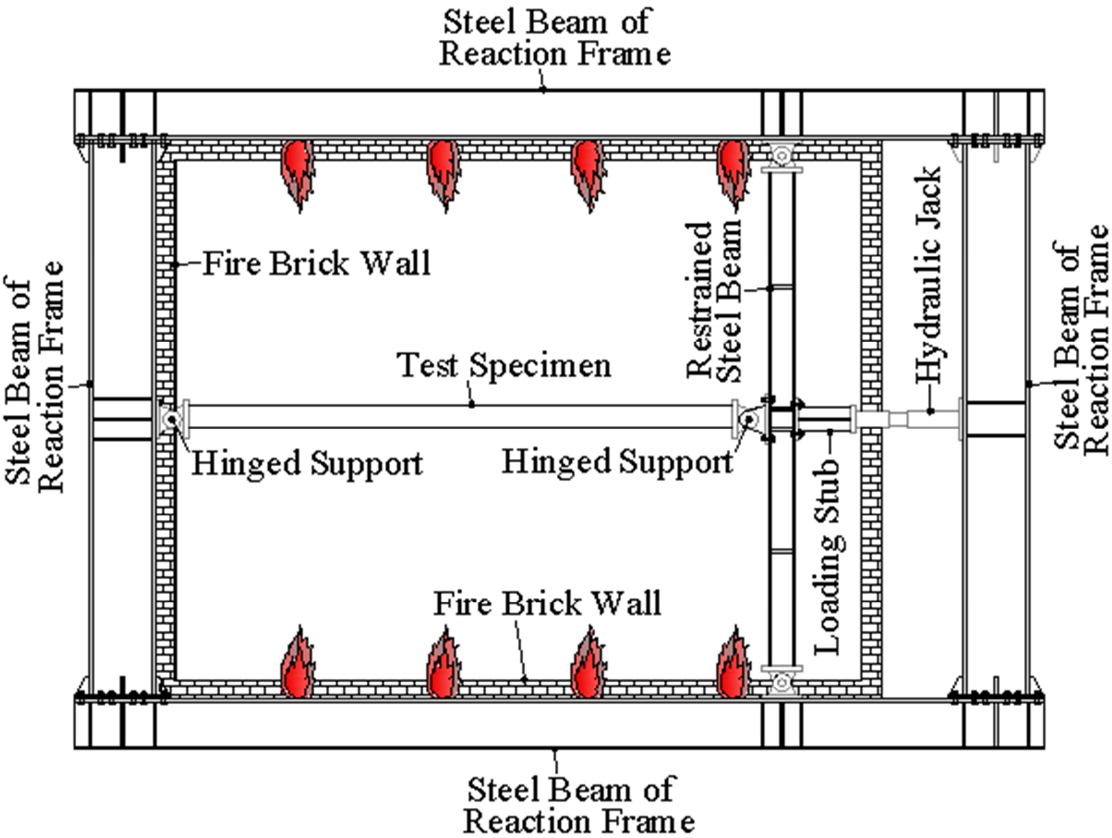

Steel Beam of Reaction Frame
Fire Brick Wall
Restrained Steel Beam
Hydraulic Jack
Steel Beam of Reaction Frame
Steel Beam of Reaction Frame
Test Specimen
Hinged Support
Hinged Support
Loading Stub
Fire Brick Wall
Steel Beam of Reaction Frame

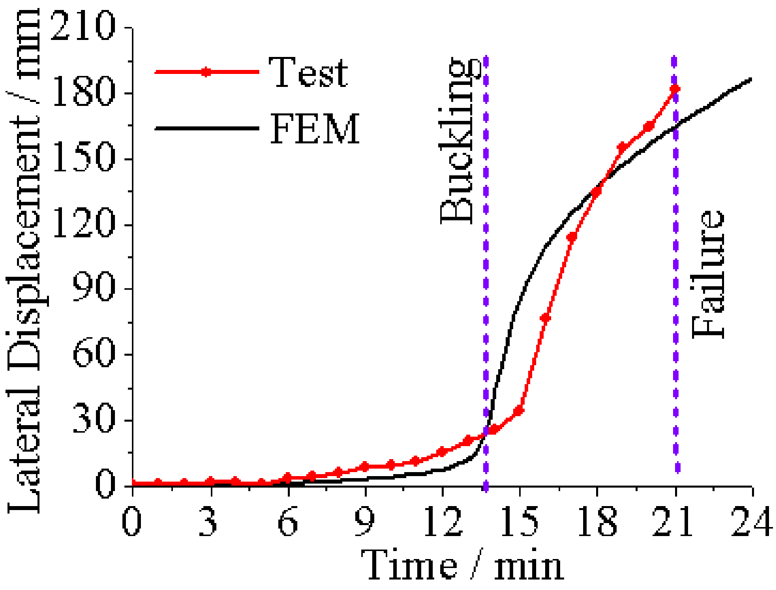

Lateral Displacement / mm
210
180
150
120
90
60
30
0
Test
FEM
Buckling
Failure
0
3
6
9
12
15
18
21
24
Time / min

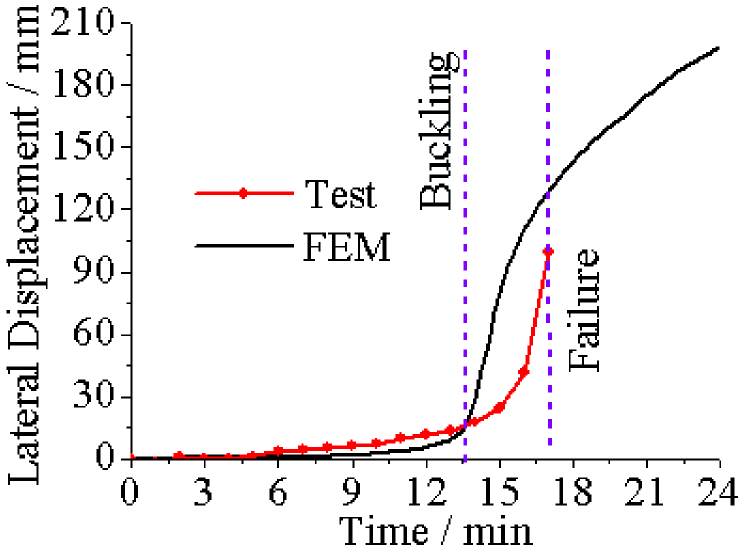

Lateral Displacement / mm
210
180
150
120
90
60
30
0
0
3
6
9
12
15
18
21
24
Time / min
Test
FEM
Buckling
Failure

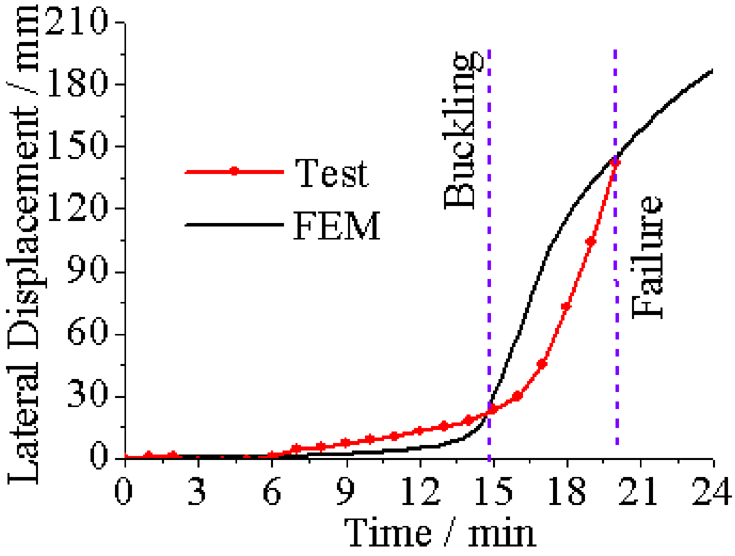

Lateral Displacement / mm
210
180
150
120
90
60
30
0
0
3
6
9
12
15
18
21
24
Time / min
Test
FEM
Buckling
Failure

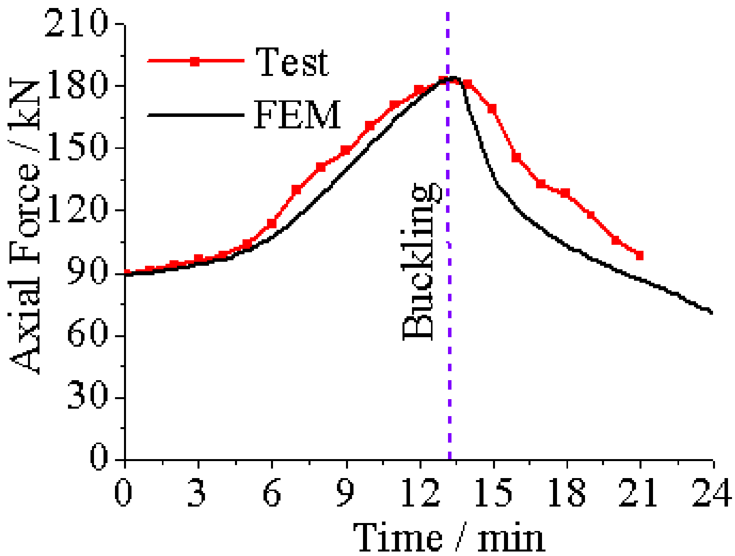

Axial Force / kN
210
180
150
120
90
60
30
0
Test
FEM
Buckling
0
3
6
9
12
15
18
21
24
Time / min

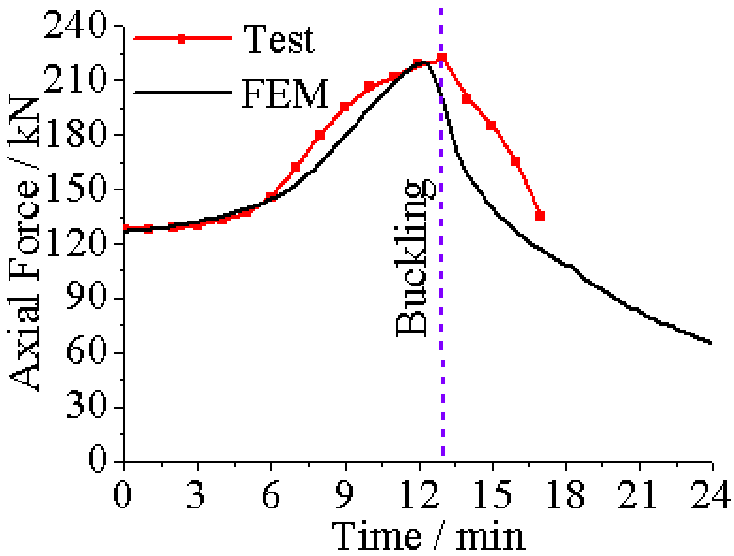

Test
FEM
Buckling
Axial Force / kN
Time / min
240
210
180
150
120
90
60
30
0
0
3
6
9
12
15
18
21
24

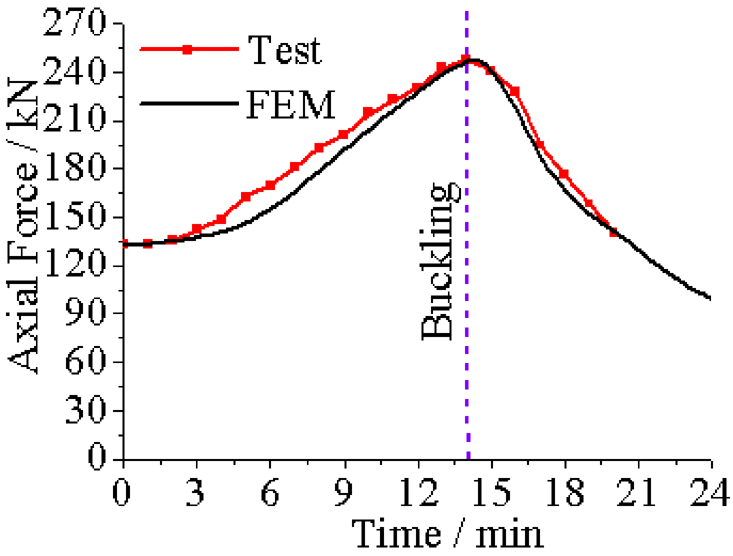

Test
FEM
Buckling
Axial Force / kN
Time / min
0
30
60
90
120
150
180
210
240
270
0
3
6
9
12
15
18
21
24

Test result

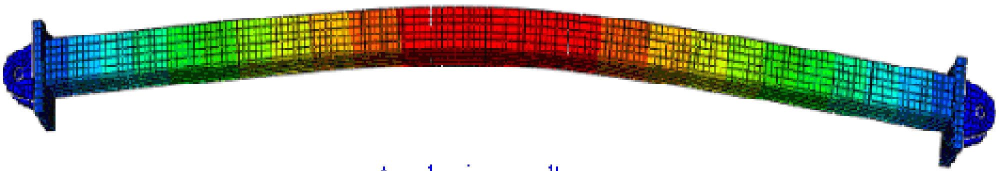

Analysis result

Test result

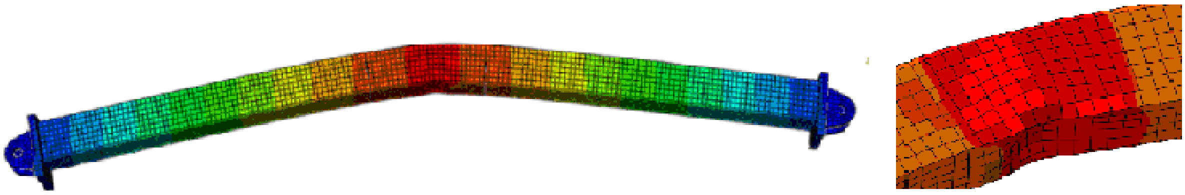

Analysis result

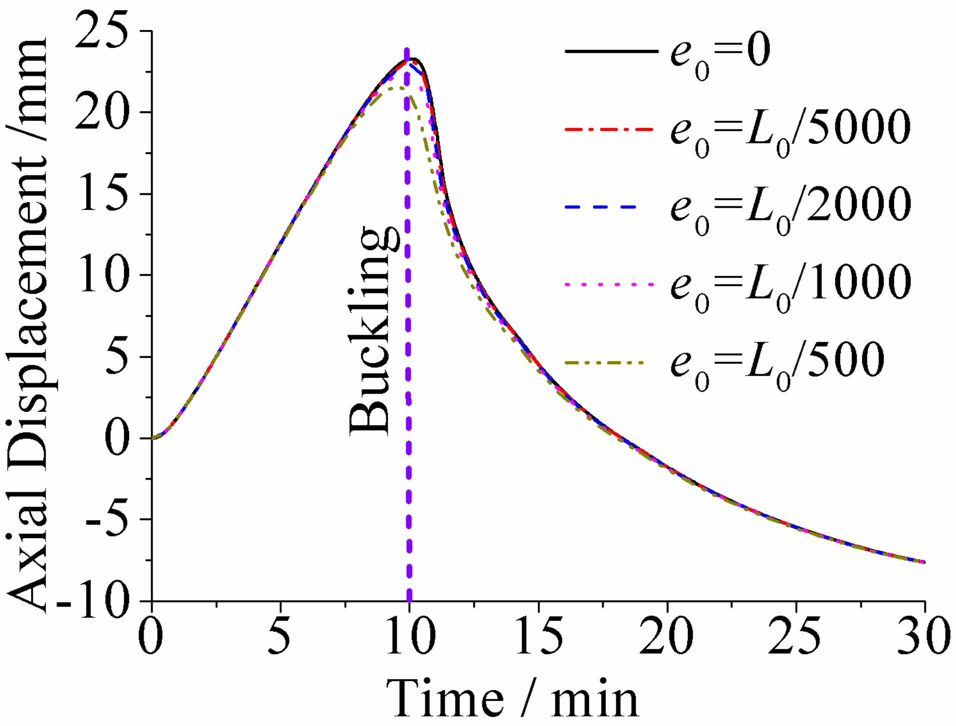

Axial Displacement /mm
Time / min
Buckling
e_0=0
e_0=L_0/5000
e_0=L_0/2000
e_0=L_0/1000
e_0=L_0/500
25
20
15
10
5
0
-5
-10
0
5
10
15
20
25
30

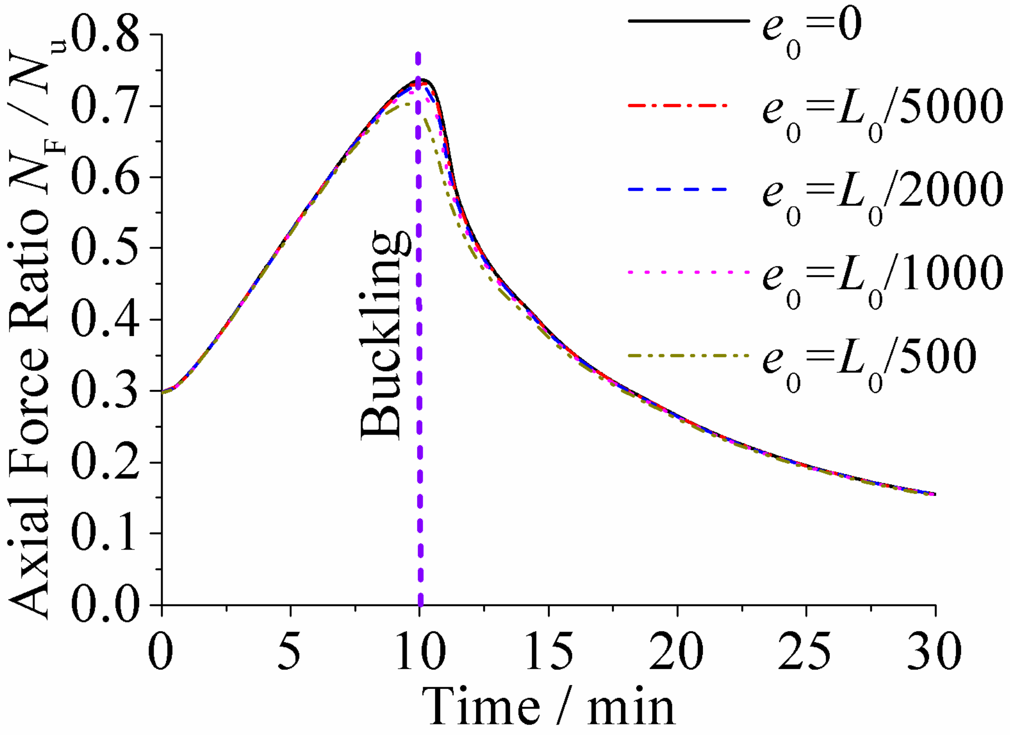

Axial Force Ratio N_F / N_u
0.0
0.1
0.2
0.3
0.4
0.5
0.6
0.7
0.8
0
5
10
15
20
25
30
Time / min
Buckling
e_0=0
e_0=L_0/5000
e_0=L_0/2000
e_0=L_0/1000
e_0=L_0/500

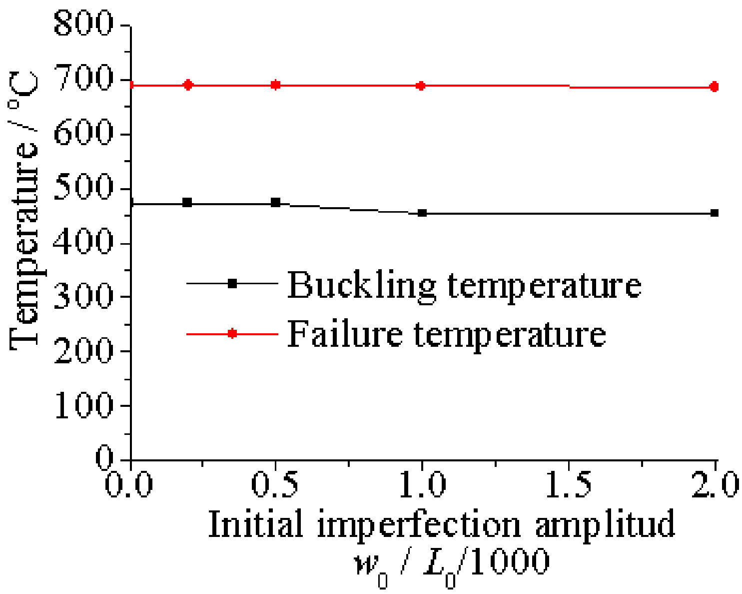

Temperature / °C
800
700
600
500
400
300
200
100
0
0.0
0.5
1.0
1.5
2.0
Buckling temperature
Failure temperature
Initial imperfection amplitud
w0 / L0/1000

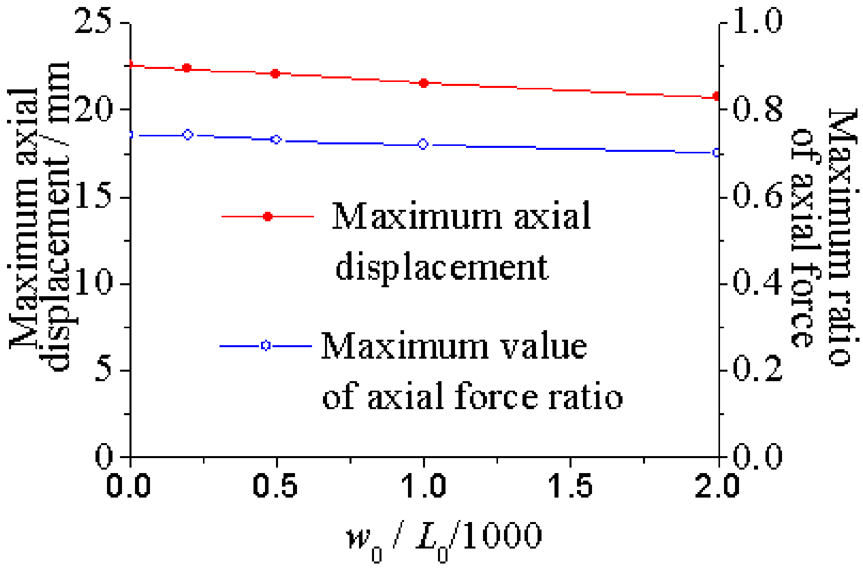

Maximum axial displacement / mm
Maximum ratio of axial force
Maximum axial displacement
Maximum value of axial force ratio
25
20
15
10
5
0
1.0
0.8
0.6
0.4
0.2
0.0
0.0
0.5
1.0
1.5
2.0
w0 / L0/1000

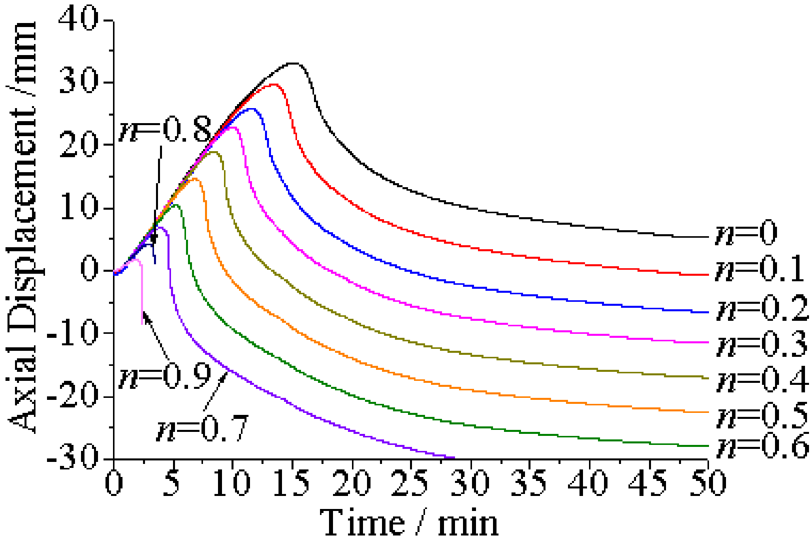

40
30
20
10
0
-10
-20
-30
Axial Displacement /mm
0
5
10
15
20
25
30
35
40
45
50
Time / min
n=0.8
n=0.9
n=0.7
n=0
n=0.1
n=0.2
n=0.3
n=0.4
n=0.5
n=0.6

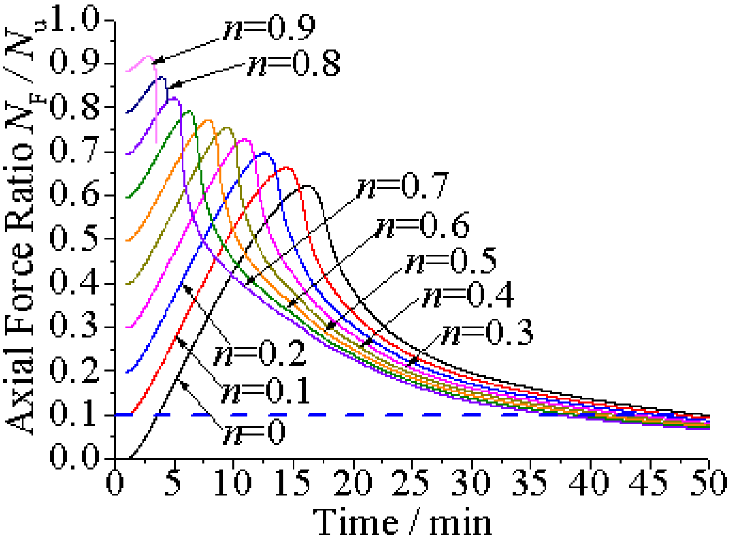
Axial Force Ratio N_F / N_u
1.0
0.9
0.8
0.7
0.6
0.5
0.4
0.3
0.2
0.1
0.0
0 5 10 15 20 25 30 35 40 45 50
Time / min
n=0.9
n=0.8
n=0.7
n=0.6
n=0.5
n=0.4
n=0.3
n=0.2
n=0.1
n=0

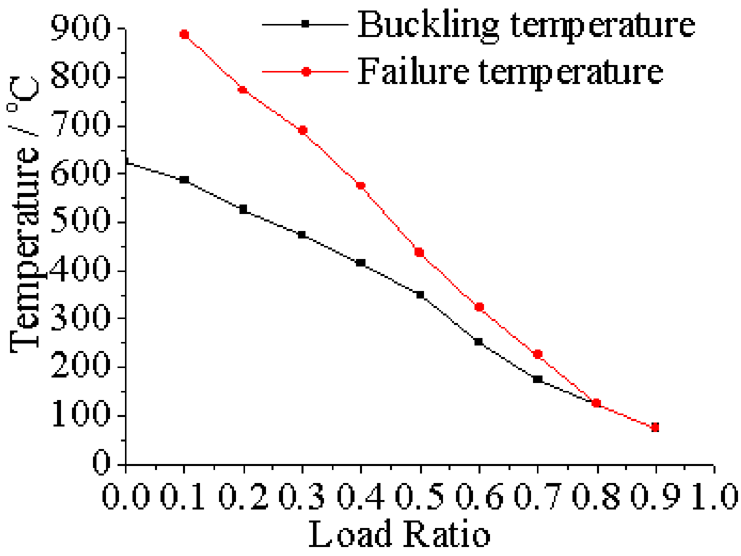
Buckling temperature
Failure temperature
Temperature / °C
900
800
700
600
500
400
300
200
100
0
0.0 0.1 0.2 0.3 0.4 0.5 0.6 0.7 0.8 0.9 1.0
Load Ratio

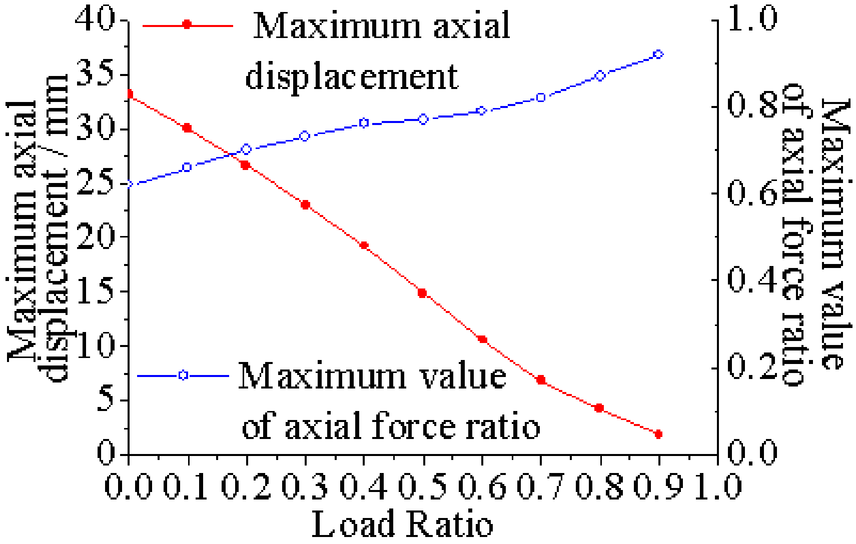
Maximum axial displacement
Maximum value of axial force ratio
Maximum axial displacement / mm
Maximum value of axial force ratio
Load Ratio
0.0 0.1 0.2 0.3 0.4 0.5 0.6 0.7 0.8 0.9 1.0
0 5 10 15 20 25 30 35 40
0.0 0.2 0.4 0.6 0.8 1.0

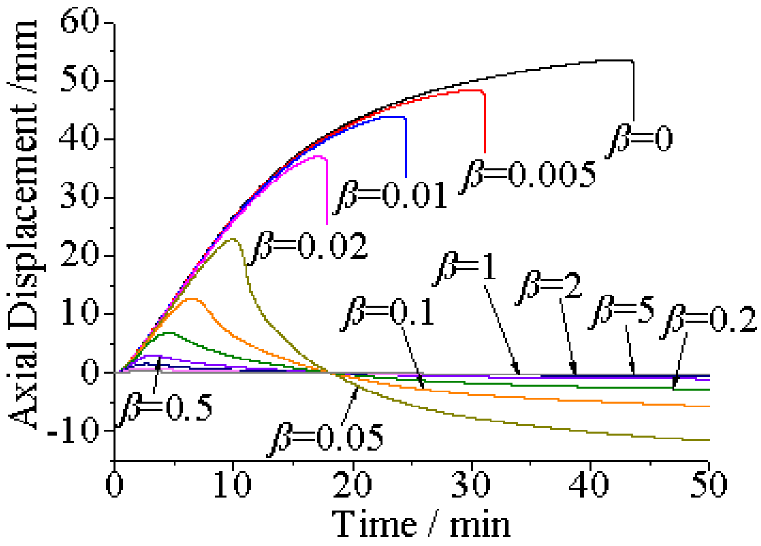

Axial Displacement /mm
Time / min
60
50
40
30
20
10
0
-10
0
10
20
30
40
50
β=0
β=0.005
β=0.01
β=0.02
β=1
β=2
β=5
β=0.2
β=0.1
β=0.5
β=0.05

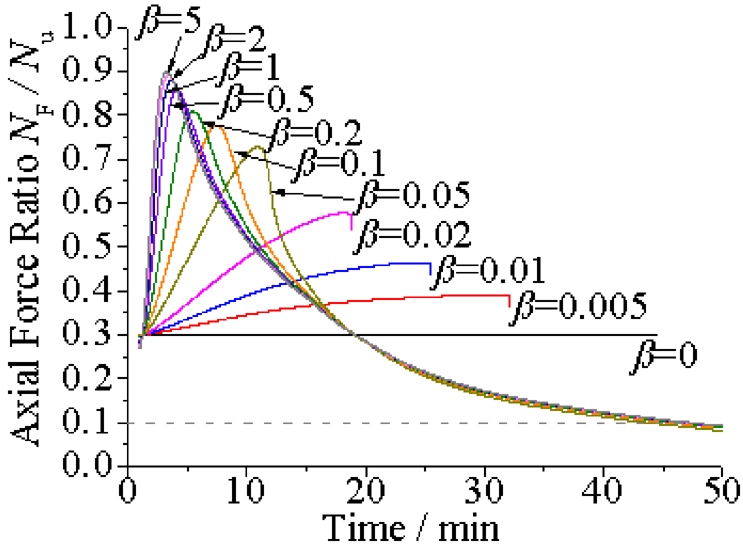

Axial Force Ratio N_F / N_u
Time / min
β=5
β=2
β=1
β=0.5
β=0.2
β=0.1
β=0.05
β=0.02
β=0.01
β=0.005
β=0

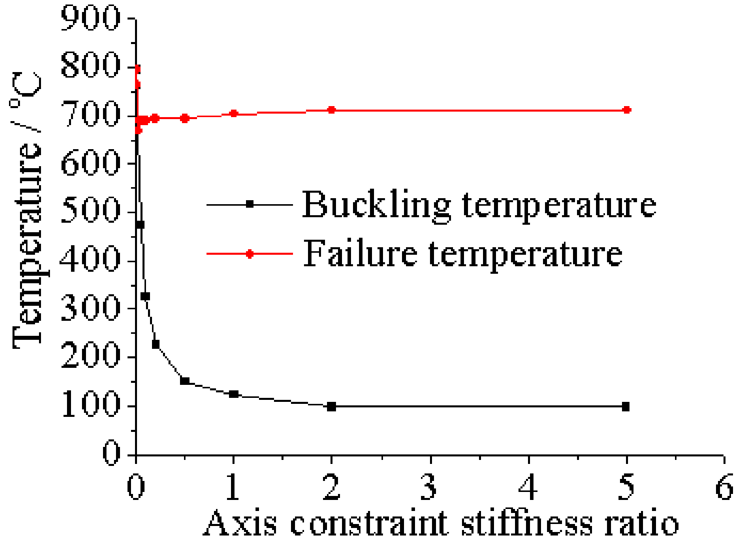

Temperature / °C
900
800
700
600
500
400
300
200
100
0
0
1
2
3
4
5
6
Axis constraint stiffness ratio
Buckling temperature
Failure temperature

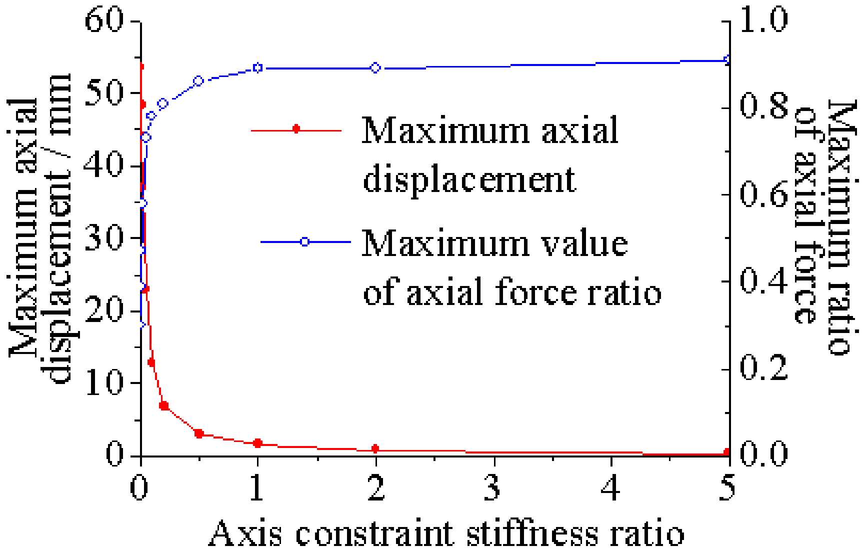
Maximum axial displacement / mm
60
50
40
30
20
10
0
0
1
2
3
4
5
Axis constraint stiffness ratio
1.0
0.8
0.6
0.4
0.2
0.0
Maximum ratio of axial force
Maximum axial displacement
Maximum value of axial force ratio

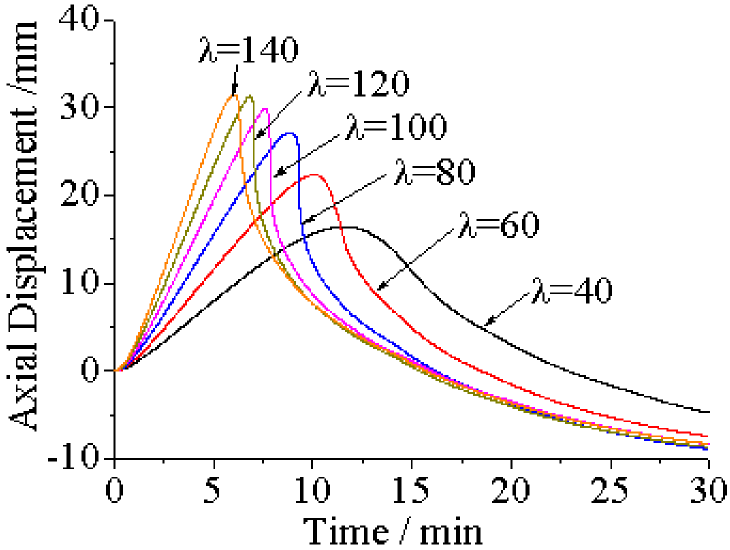

Axial Displacement /mm
Time / min
λ=140
λ=120
λ=100
λ=80
λ=60
λ=40
40
30
20
10
0
-10
0
5
10
15
20
25
30

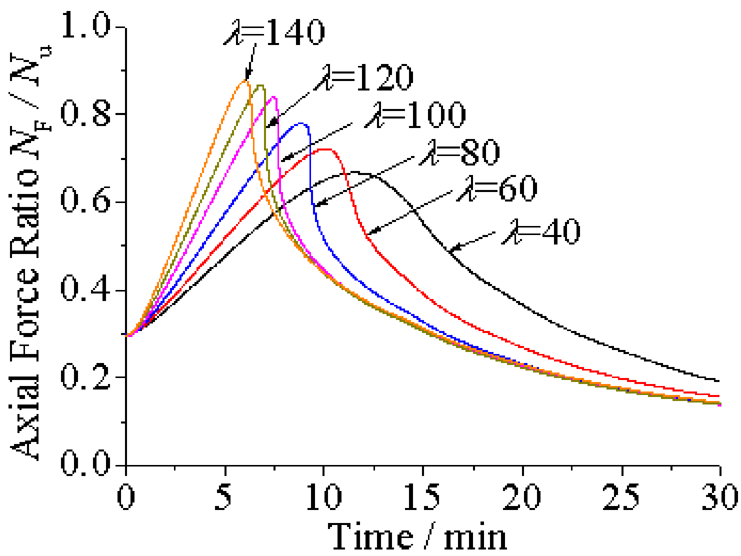
λ=140
λ=120
λ=100
λ=80
λ=60
λ=40
Axial Force Ratio N_F / N_u
0.0
0.2
0.4
0.6
0.8
1.0
0
5
10
15
20
25
30
Time / min

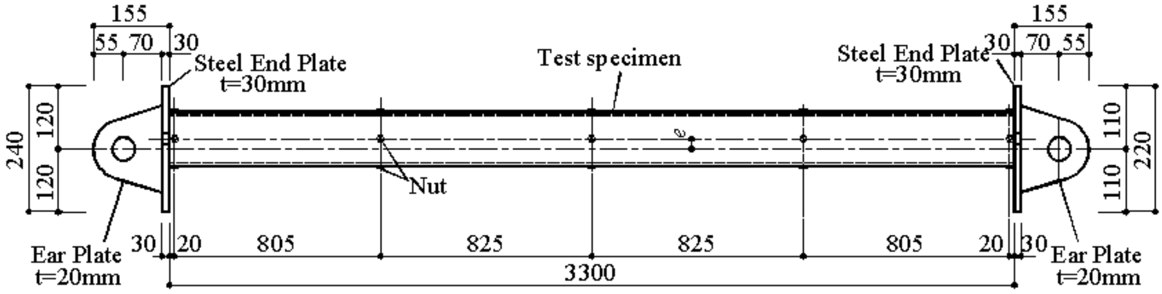
155
55 70
30
Steel End Plate
t=30mm
Test specimen
Steel End Plate
t=30mm
30 70 55
155
240
120
120
Nut
e
110
110
220
Ear Plate
t=20mm
30
20
805
825
825
805
20
30
Ear Plate
t=20mm
3300

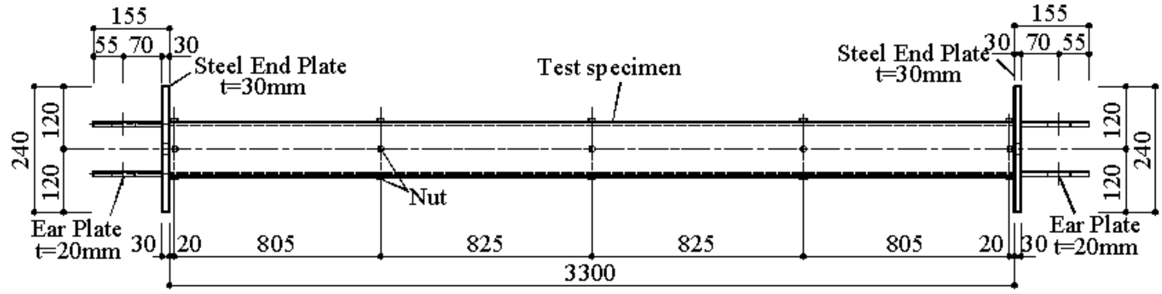
155
55 70
30
Steel End Plate
t=30mm
Test specimen
Steel End Plate
t=30mm
30 70 55
155
240
120
120
Nut
120
120
240
Ear Plate
t=20mm
30
20
805
825
825
805
20
30
Ear Plate
t=20mm
3300

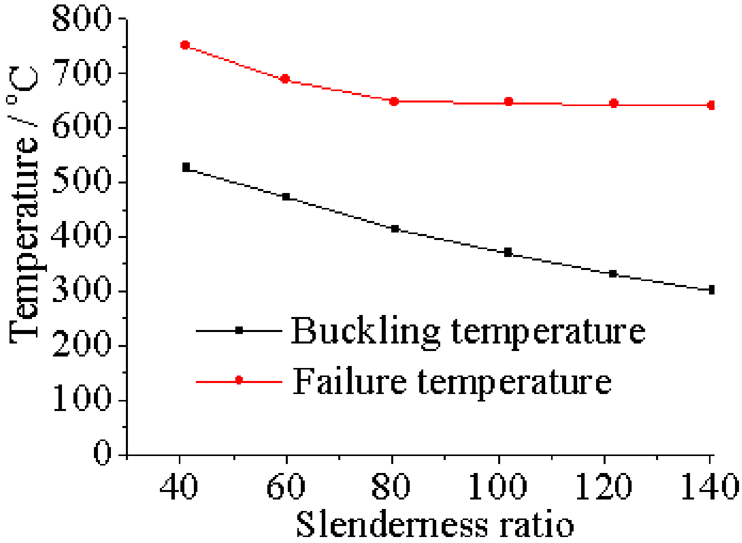

800
700
600
500
400
300
200
100
0
Temperature / °C
Buckling temperature
Failure temperature
40
60
80
100
120
140
Slenderness ratio

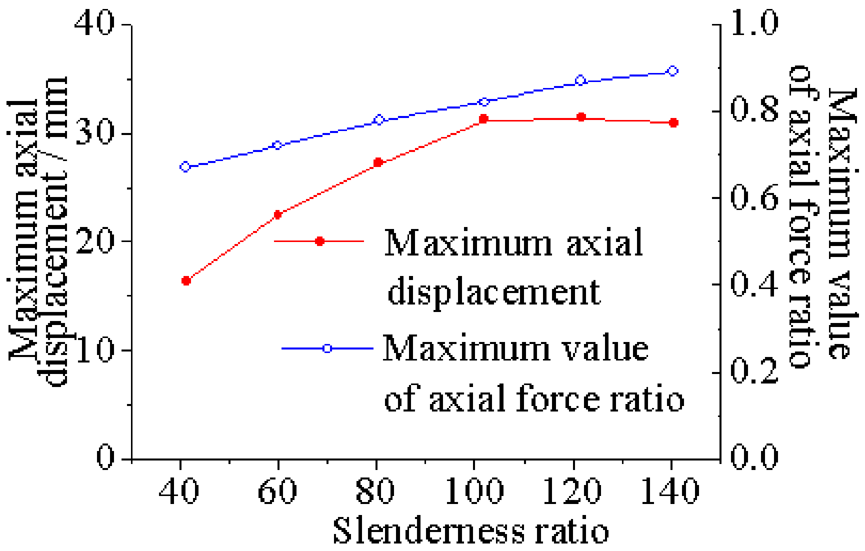
40
30
20
10
0
Maximum axial displacement / mm
1.0
0.8
0.6
0.4
0.2
0.0
Maximum value of axial force ratio
Maximum axial displacement
Maximum value of axial force ratio
40
60
80
100
120
140
Slenderness ratio

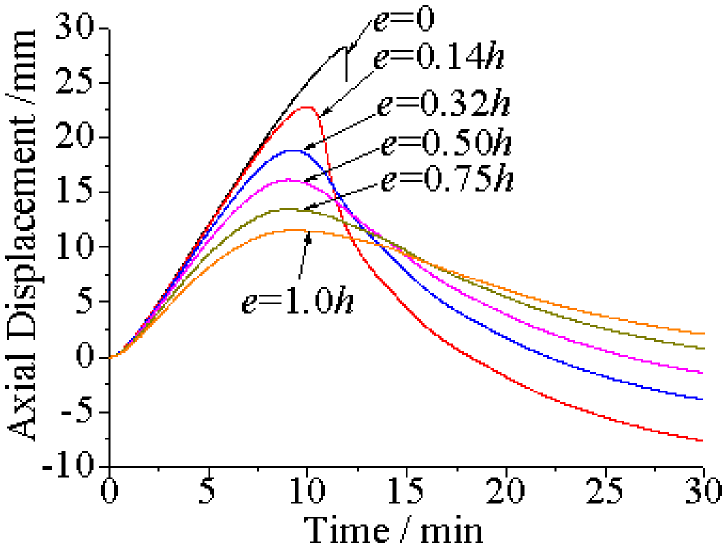

e=0
e=0.14h
e=0.32h
e=0.50h
e=0.75h
e=1.0h
Axial Displacement /mm
30
25
20
15
10
5
0
-5
-10
0
5
10
15
20
25
30
Time / min

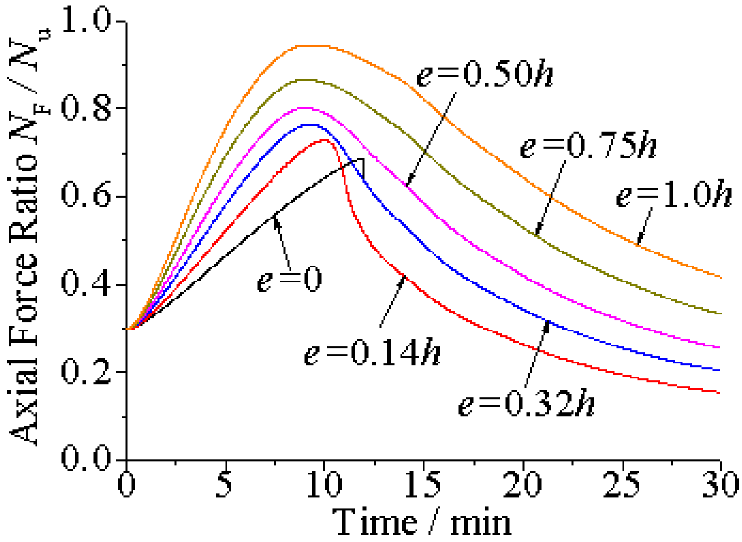

Axial Force Ratio N_F / N_u
1.0
0.8
0.6
0.4
0.2
0.0
0
5
10
15
20
25
30
Time / min
e=0.50h
e=0.75h
e=1.0h
e=0
e=0.14h
e=0.32h

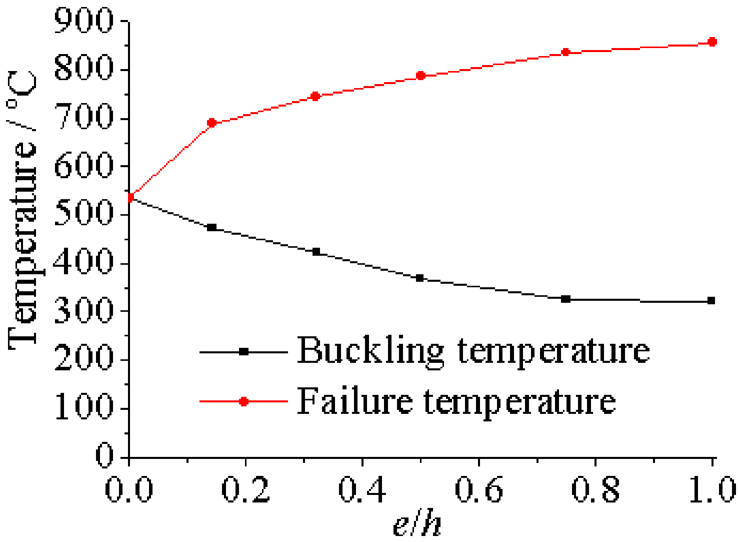
Temperature / °C
900
800
700
600
500
400
300
200
100
0
0.0
0.2
0.4
0.6
0.8
1.0
e/h
Buckling temperature
Failure temperature

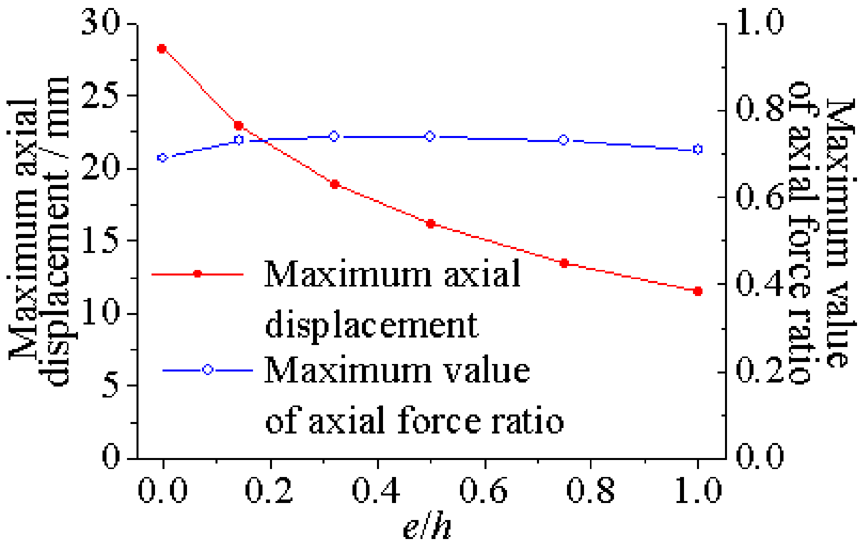

Maximum axial displacement / mm
30
25
20
15
10
5
0
0.0
0.2
0.4
0.6
0.8
1.0
e/h
Maximum value of axial force ratio
1.0
0.8
0.6
0.4
0.2
0.0
Maximum axial displacement
Maximum value of axial force ratio

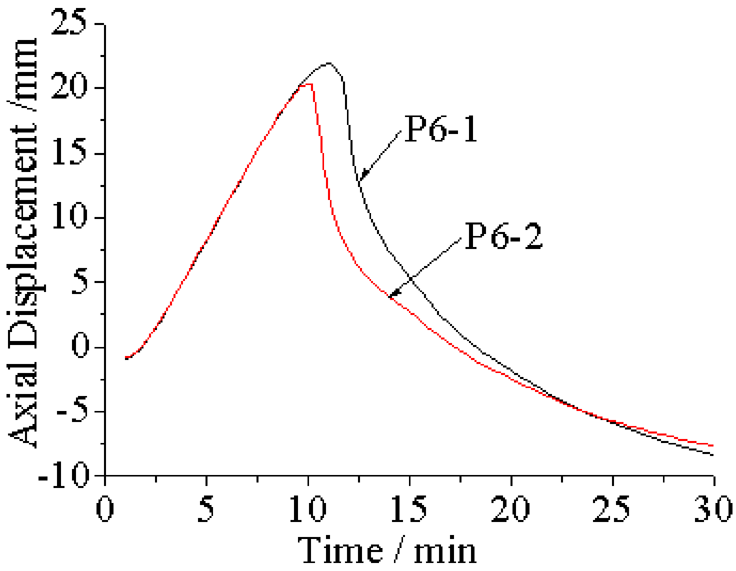

Axial Displacement /mm
25
20
15
10
5
0
-5
-10
0
5
10
15
20
25
30
Time / min
P6-1
P6-2

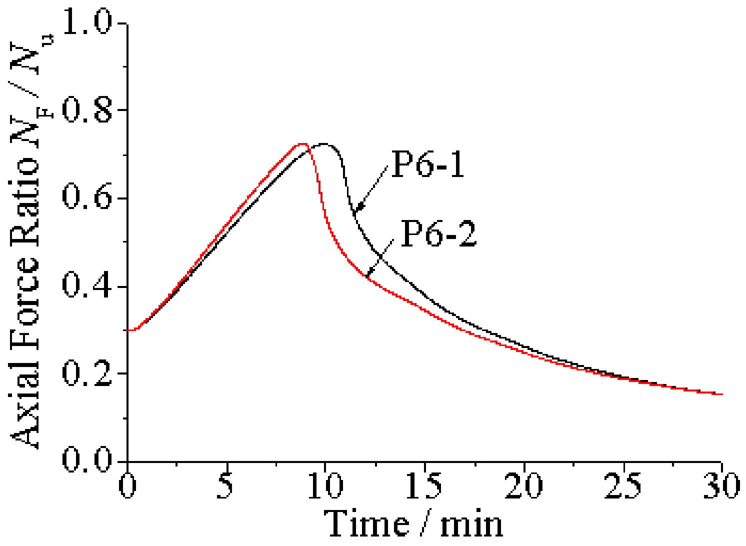
Axial Force Ratio N_F / N_u
1.0
0.8
0.6
0.4
0.2
0.0
0
5
10
15
20
25
30
Time / min
P6-1
P6-2

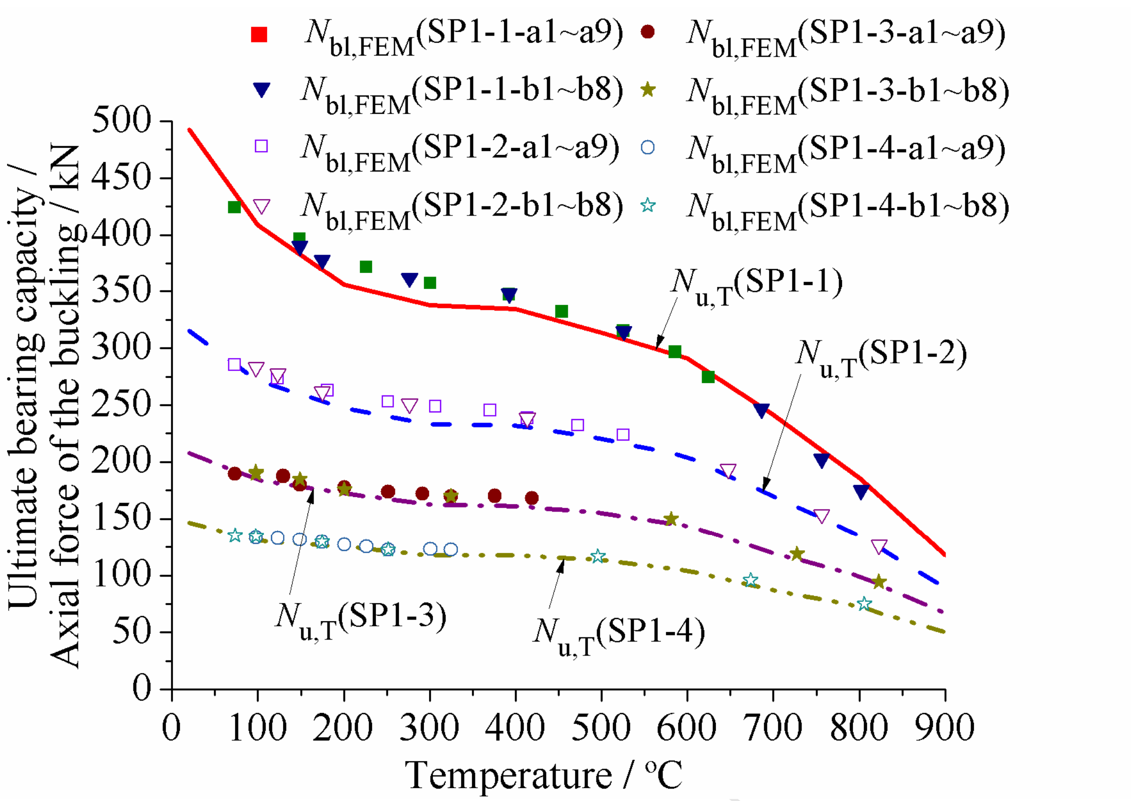

$N_{bl,FEM}$(SP1-1-a1~a9)
$N_{bl,FEM}$(SP1-3-a1~a9)
$N_{bl,FEM}$(SP1-1-b1~b8)
$N_{bl,FEM}$(SP1-3-b1~b8)
$N_{bl,FEM}$(SP1-2-a1~a9)
$N_{bl,FEM}$(SP1-4-a1~a9)
$N_{bl,FEM}$(SP1-2-b1~b8)
$N_{bl,FEM}$(SP1-4-b1~b8)
$N_{u,T}$(SP1-1)
$N_{u,T}$(SP1-2)
$N_{u,T}$(SP1-3)
$N_{u,T}$(SP1-4)
Ultimate bearing capacity /
Axial force of the buckling / kN
0
50
100
150
200
250
300
350
400
450
500
0
100
200
300
400
500
600
700
800
900
Temperature / °C

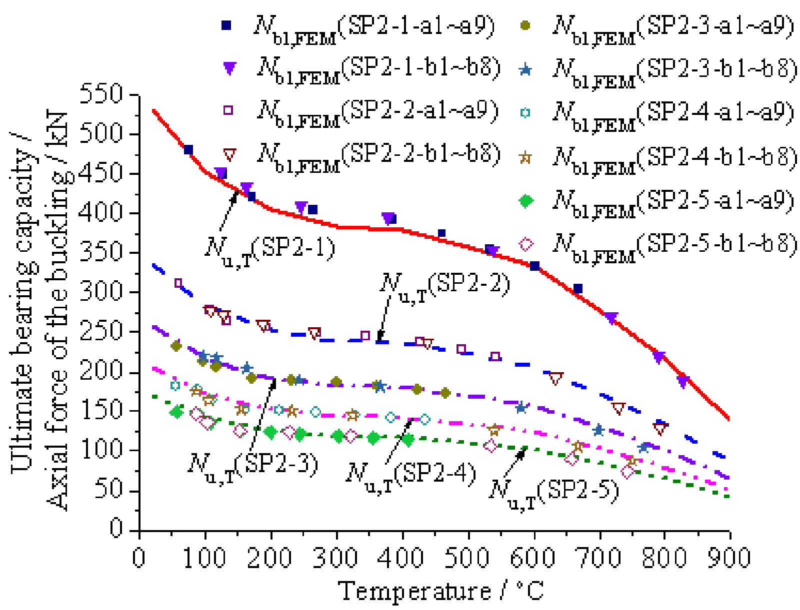
$N_{b1,FEM}$(SP2-1-a1~a9)
$N_{b1,FEM}$(SP2-1-b1~b8)
$N_{b1,FEM}$(SP2-2-a1~a9)
$N_{b1,FEM}$(SP2-2-b1~b8)
$N_{b1,FEM}$(SP2-3-a1~a9)
$N_{b1,FEM}$(SP2-3-b1~b8)
$N_{b1,FEM}$(SP2-4-a1~a9)
$N_{b1,FEM}$(SP2-4-b1~b8)
$N_{b1,FEM}$(SP2-5-a1~a9)
$N_{b1,FEM}$(SP2-5-b1~b8)
$N_{u,T}$(SP2-1)
$N_{u,T}$(SP2-2)
$N_{u,T}$(SP2-3)
$N_{u,T}$(SP2-4)
$N_{u,T}$(SP2-5)
Ultimate bearing capacity / Axial force of the buckling / kN
Temperature / °C
0
50
100
150
200
250
300
350
400
450
500
550
600
700
800
900

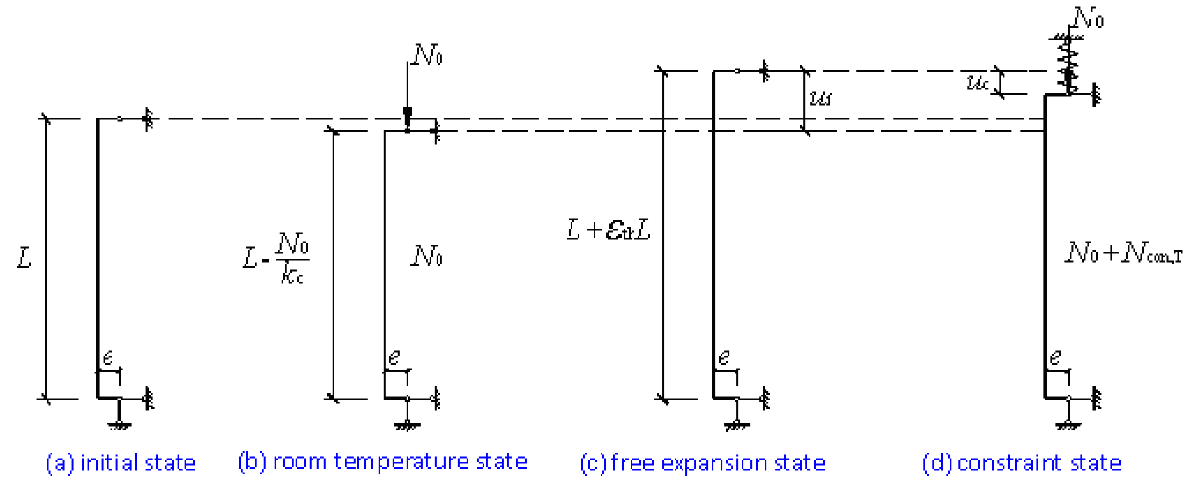
N0
N0
u_f
u_c
N0
L
L - N0/kc
N0
L + ε_th L
N0 + N_con,T
e
e
e
e
(a) initial state
(b) room temperature state
(c) free expansion state
(d) constraint state

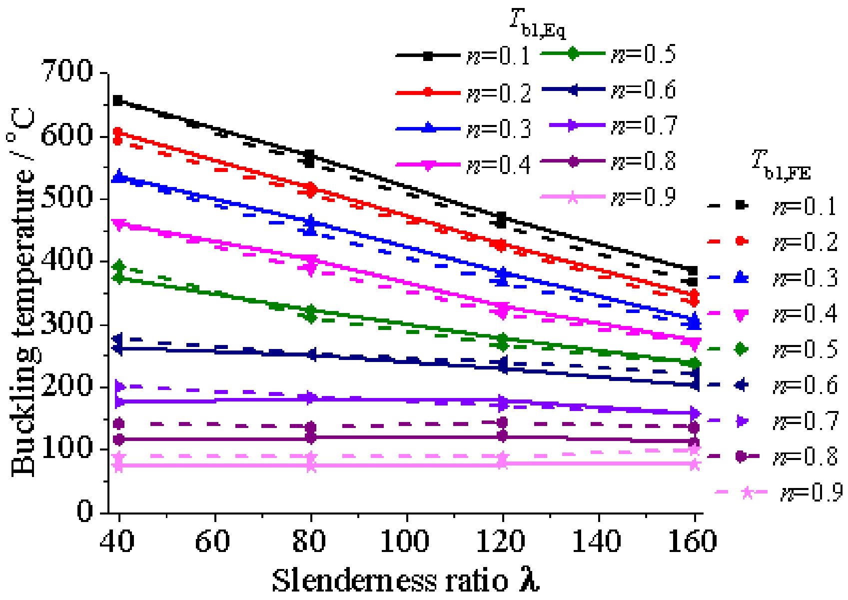

$T_{b1,Eq}$
n=0.1
n=0.2
n=0.3
n=0.4
n=0.5
n=0.6
n=0.7
n=0.8
n=0.9
$T_{b1,FE}$
n=0.1
n=0.2
n=0.3
n=0.4
n=0.5
n=0.6
n=0.7
n=0.8
n=0.9
Buckling temperature / °C
0
100
200
300
400
500
600
700
40
60
80
100
120
140
160
Slenderness ratio λ

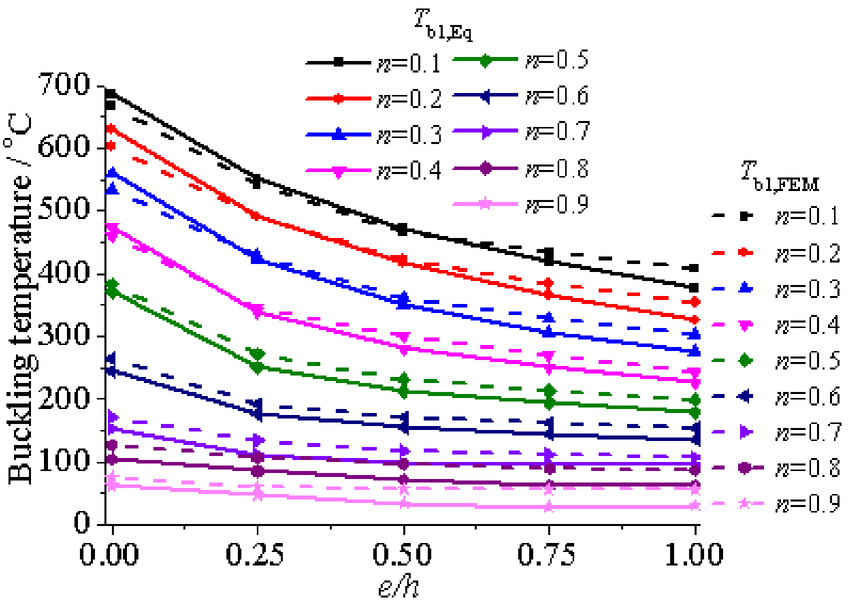

$T_{b1,Eq}$
n=0.1
n=0.2
n=0.3
n=0.4
n=0.5
n=0.6
n=0.7
n=0.8
n=0.9
$T_{b1,FEM}$
n=0.1
n=0.2
n=0.3
n=0.4
n=0.5
n=0.6
n=0.7
n=0.8
n=0.9
Buckling temperature / °C
0
100
200
300
400
500
600
700
0.00
0.25
0.50
0.75
1.00
e/h

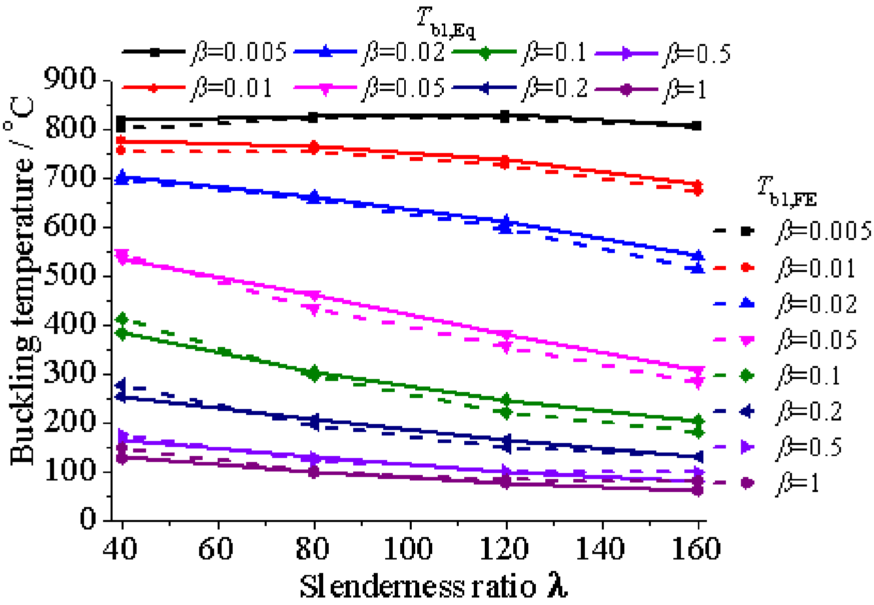

$T_{b1,Eq}$
β=0.005
β=0.02
β=0.1
β=0.5
β=0.01
β=0.05
β=0.2
β=1
$T_{b1,FE}$
β=0.005
β=0.01
β=0.02
β=0.05
β=0.1
β=0.2
β=0.5
β=1
Buckling temperature / °C
Slenderness ratio λ
0
100
200
300
400
500
600
700
800
900
40
60
80
100
120
140
160

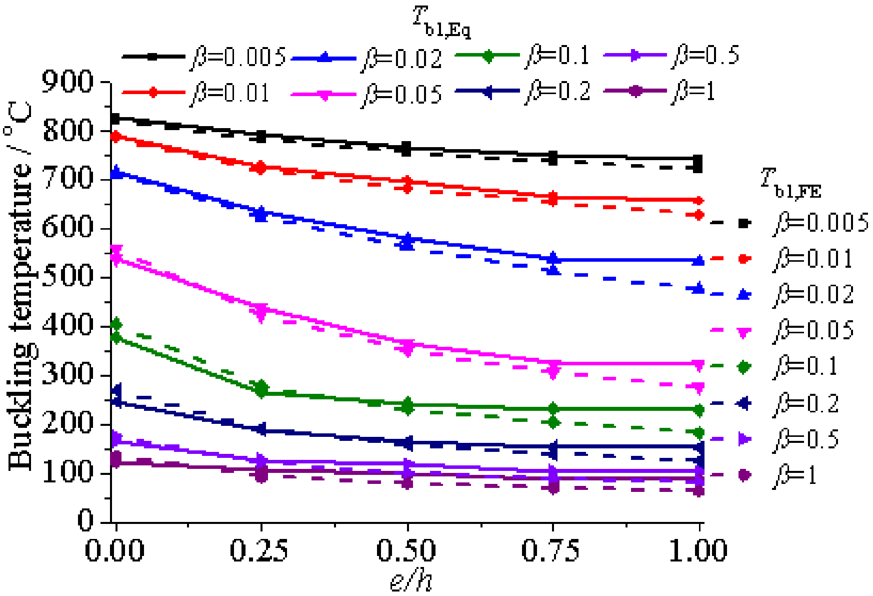

$T_{b1,Eq}$
β=0.005
β=0.02
β=0.1
β=0.5
β=0.01
β=0.05
β=0.2
β=1
$T_{b1,FE}$
β=0.005
β=0.01
β=0.02
β=0.05
β=0.1
β=0.2
β=0.5
β=1
Buckling temperature / °C
0
100
200
300
400
500
600
700
800
900
0.00
0.25
0.50
0.75
1.00
e/h

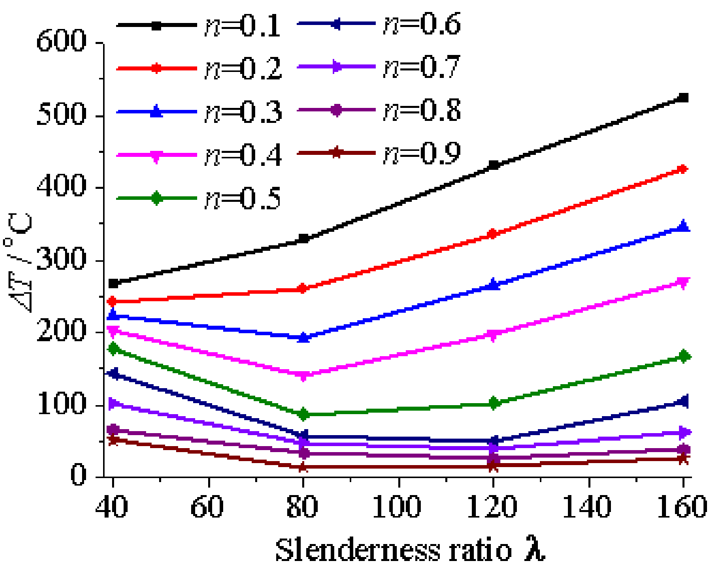

n=0.1
n=0.2
n=0.3
n=0.4
n=0.5
n=0.6
n=0.7
n=0.8
n=0.9
ΔT / °C
600
500
400
300
200
100
0
40
60
80
100
120
140
160
Slenderness ratio λ

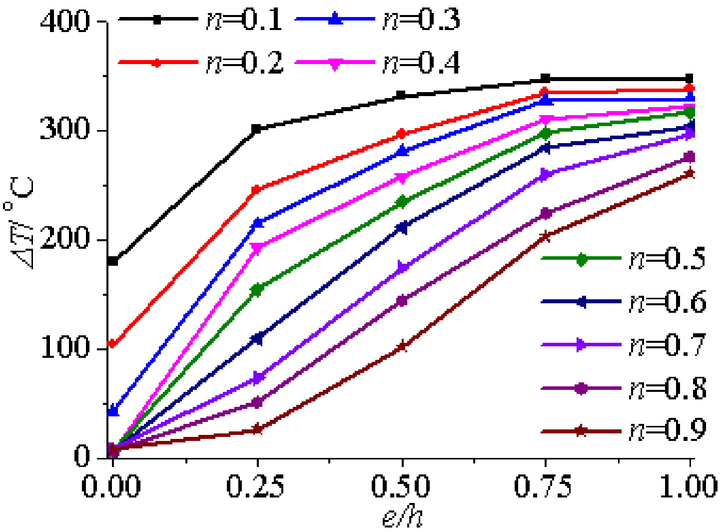

400
300
200
100
0
ΔT/ °C
n=0.1
n=0.2
n=0.3
n=0.4
n=0.5
n=0.6
n=0.7
n=0.8
n=0.9
0.00
0.25
0.50
0.75
1.00
e/h

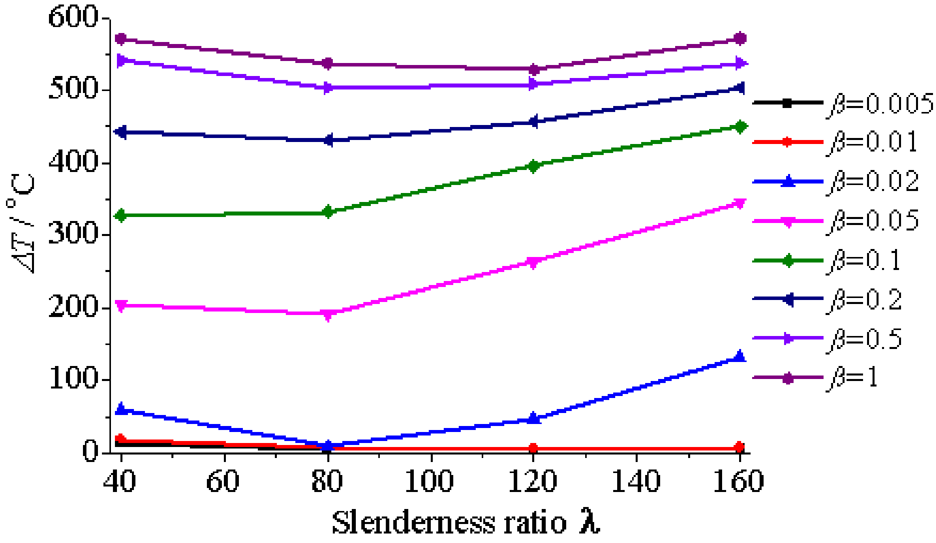
600
500
400
300
200
100
0
ΔT / °C
40
60
80
100
120
140
160
Slenderness ratio λ
β=0.005
β=0.01
β=0.02
β=0.05
β=0.1
β=0.2
β=0.5
β=1

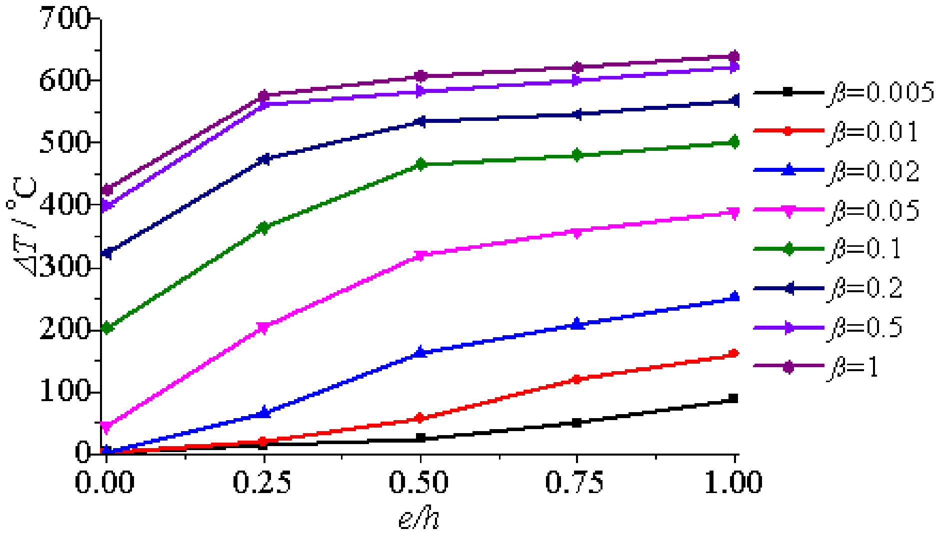
700
600
500
400
300
200
100
0
ΔT / °C
0.00
0.25
0.50
0.75
1.00
e/h
β=0.005
β=0.01
β=0.02
β=0.05
β=0.1
β=0.2
β=0.5
β=1

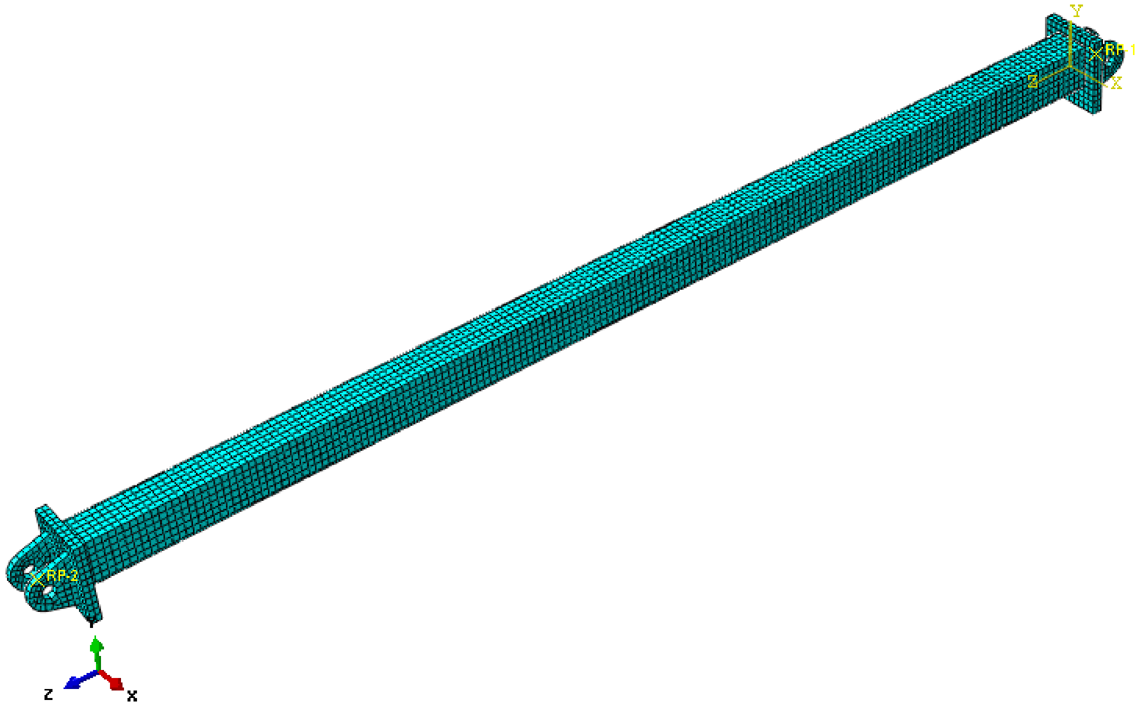
RP-1
RP-2
Y
Z
X

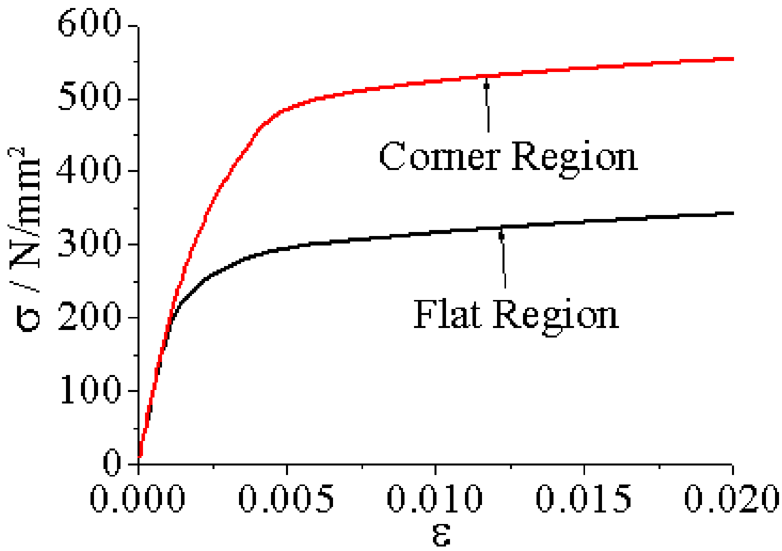
600
500
400
300
200
100
0
σ / N/mm²
0.000
0.005
0.010
0.015
0.020
ε
Corner Region
Flat Region

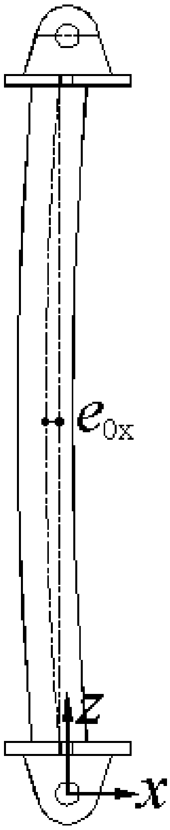
e_{0x}
z
x

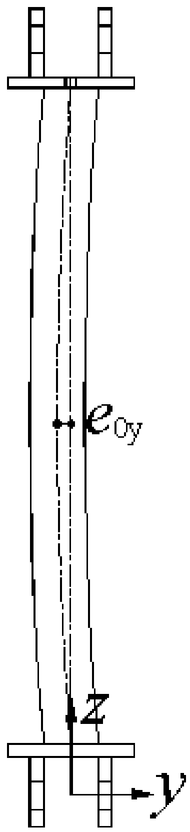
e_{0y}
z
y

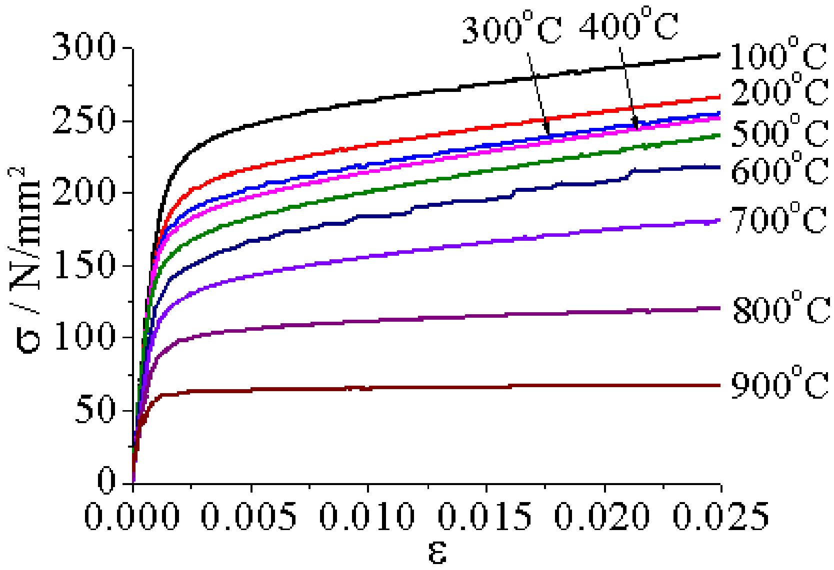

300°C 400°C
100°C
200°C
500°C
600°C
700°C
800°C
900°C
σ / N/mm²
300
250
200
150
100
50
0
0.000 0.005 0.010 0.015 0.020 0.025
ε

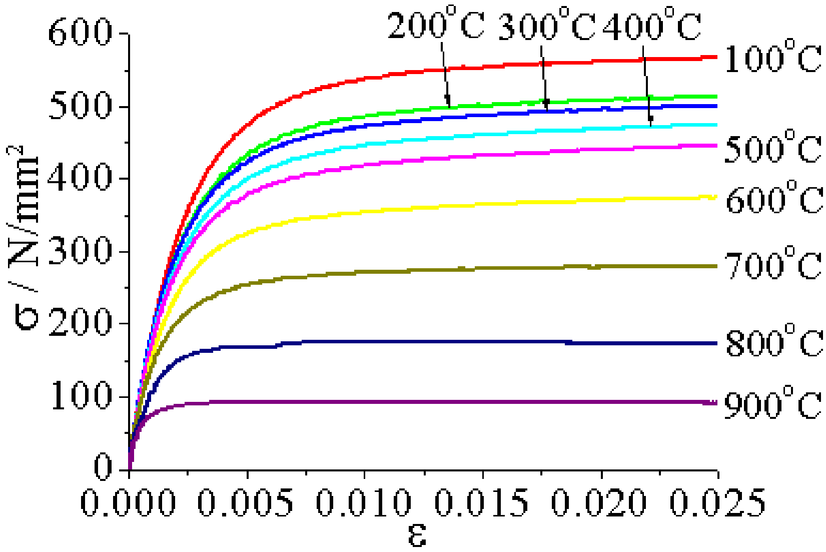
600
500
400
300
200
100
0
σ / N/mm²
0.000 0.005 0.010 0.015 0.020 0.025
ε
200°C 300°C 400°C
100°C
500°C
600°C
700°C
800°C
900°C

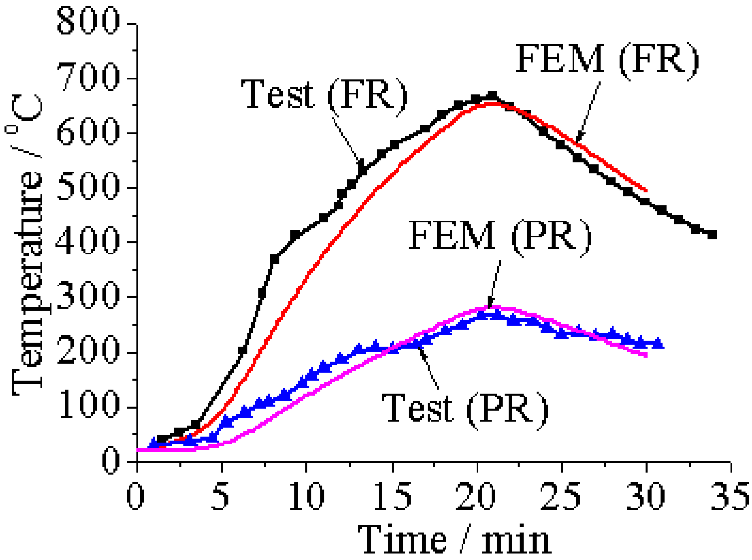

Temperature / °C
0
100
200
300
400
500
600
700
800
0
5
10
15
20
25
30
35
Time / min
Test (FR)
FEM (FR)
FEM (PR)
Test (PR)

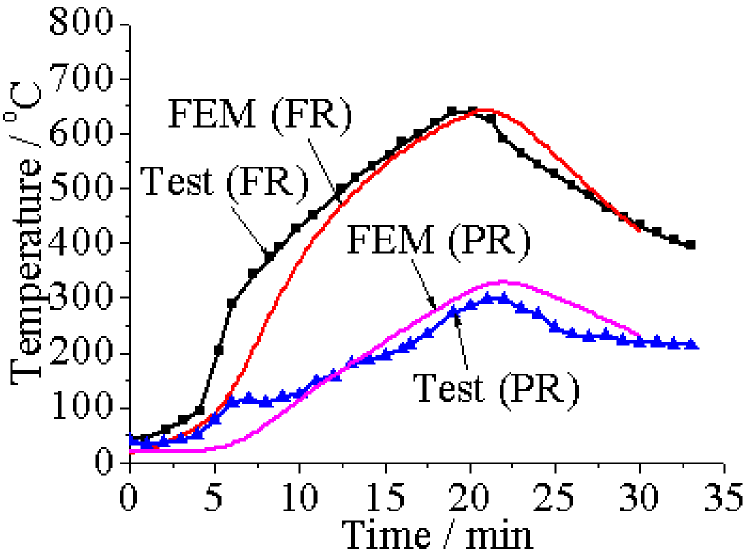

800
700
600
500
400
300
200
100
0
Temperature / °C
FEM (FR)
Test (FR)
FEM (PR)
Test (PR)
0
5
10
15
20
25
30
35
Time / min

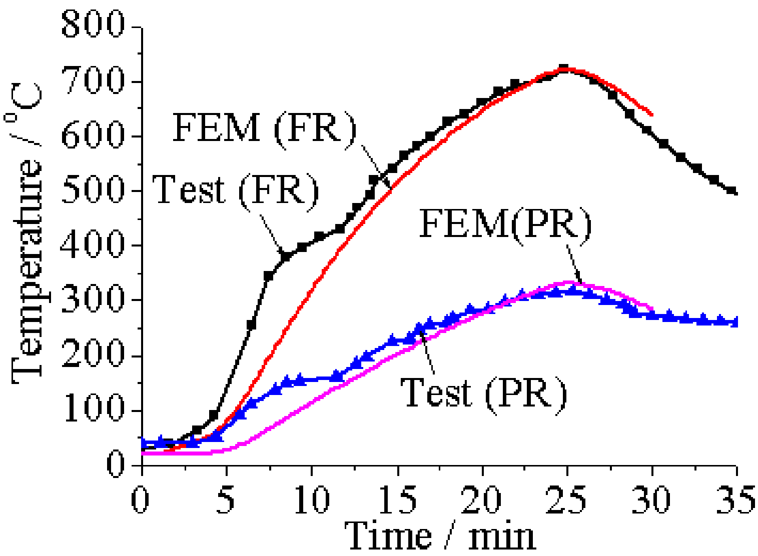

800
700
600
500
400
300
200
100
0
Temperature / °C
0
5
10
15
20
25
30
35
Time / min
FEM (FR)
Test (FR)
FEM(PR)
Test (PR)

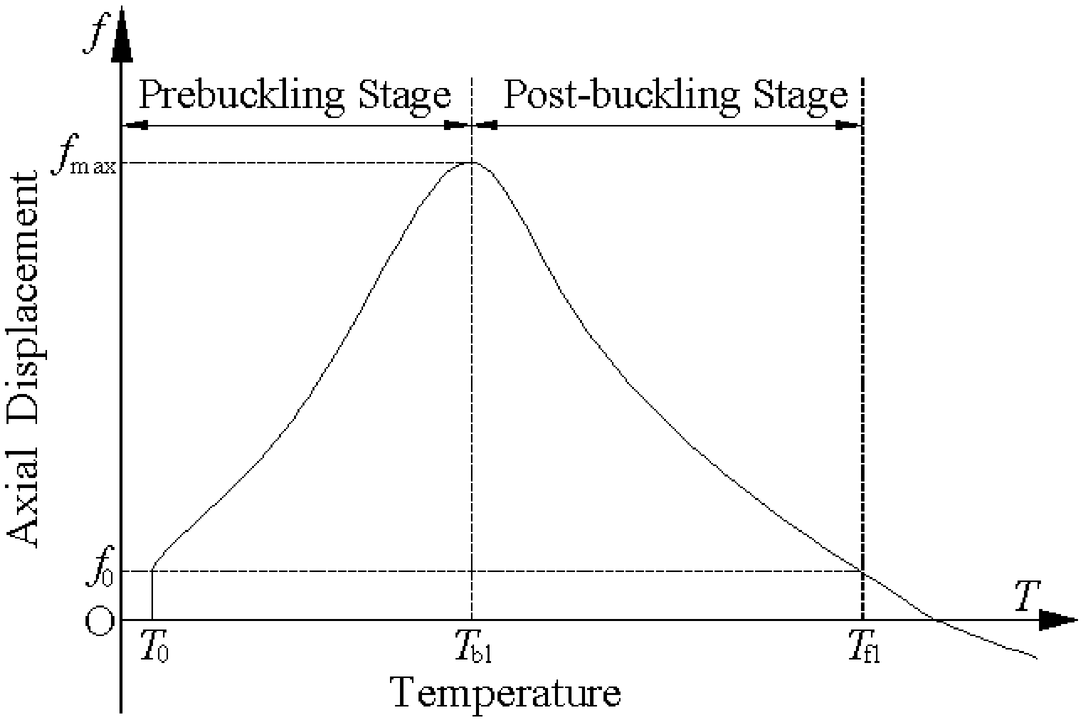
f
Prebuckling Stage
Post-buckling Stage
f max
Axial Displacement
f0
O
T0
Tb1
Tf1
T
Temperature

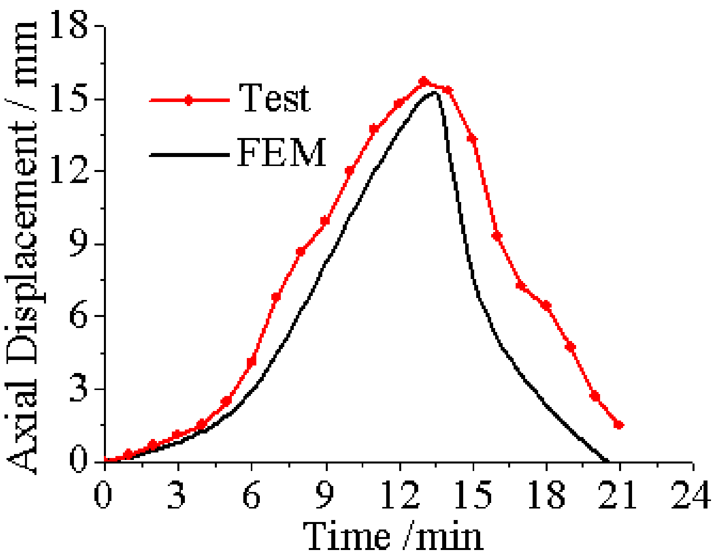
Axial Displacement / mm
18
15
12
9
6
3
0
Test
FEM
0
3
6
9
12
15
18
21
24
Time /min

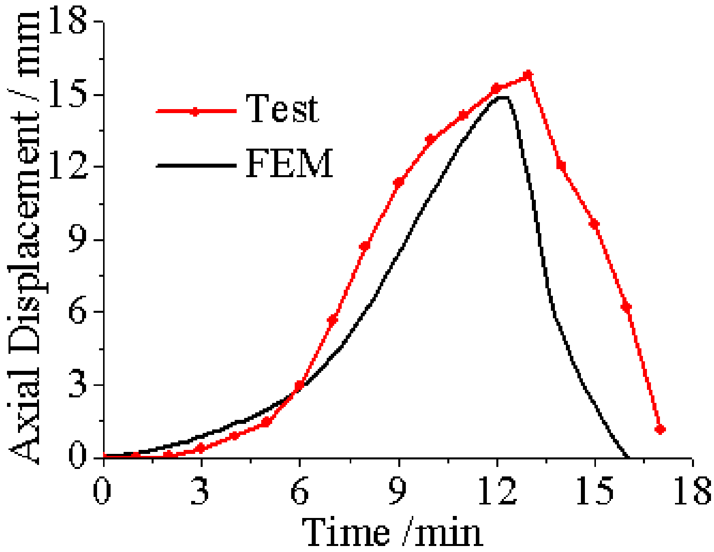

Axial Displacement / mm
0
3
6
9
12
15
18
Test
FEM
0
3
6
9
12
15
18
Time /min

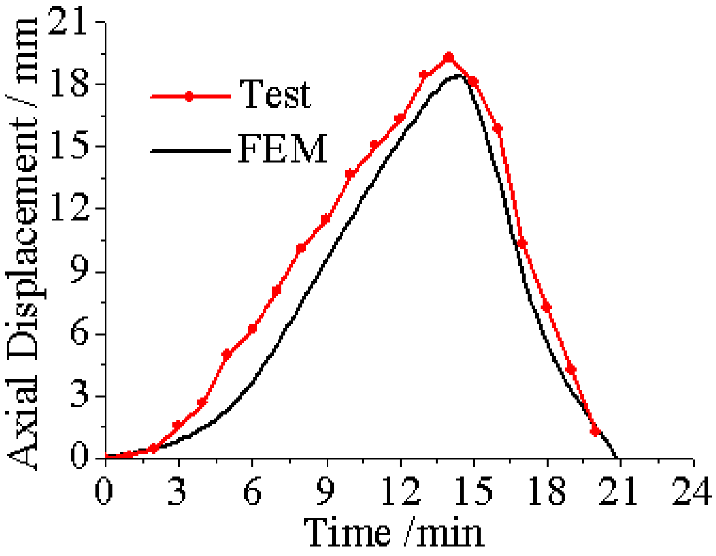

Axial Displacement / mm
0
3
6
9
12
15
18
21
Test
FEM
0
3
6
9
12
15
18
21
24
Time /min

Research Highlights

- Load ratio and axial constraint slenderness are external influence factors on the fire resistance.
- Slenderness ratio and eccentricity are internal influence factors on the fire resistance.
- The columns with constraints in fire experiences the pre-buckling stage and post-buckling stage.
- There are brittle failure mode and ductile failure mode occurred in columns in fire.
- An implicit formula for the buckling temperature is proposed.
- The relationship between buckling temperature and failure temperature is established.